US Department
of Transportation

**Federal Railroad
Administration**

Determination of Dynamic Fracture Toughness Properties of Rail Steels

Office of Research and
Development
Washington DC 20590

M.F. Kanninen
R.J. Dexter
J.W. Cardinal

Southwest Research Institute
Engineering and Materials Sciences Division
San Antonio TX 78284

DOT/FRA/ORD-87/08
DOT-TSC-FRA-87-3

November 1987
Final Report

Technical Report Documentation Page

1. Report No.	2. Government Accession No.	3. Recipient's Catalog No.
DOT/FRA/ORD-87/08	PB88 155734/AS	

4. Title and Subtitle
Determination of Dynamic Fracture Toughness Properties of Rail Steels

5. Report Date
November 1987

6. Performing Organization Code
DTS-76

7. Author(s) M.F. Kanninen, R.J. Dexter, J.W. Cardinal

8. Performing Organization Report No.
DOT-TSC-FRA-87-3

9. Performing Organization Name and Address
Southwest Research Institute*
Engineering and Materials Sciences Division
P.O. Drawer 28510
San Antonio, TX 78284

10. Work Unit No. (TRAIS)
RR719/R7001

11. Contract or Grant No.
DTRS-57-80-C-00086

12. Sponsoring Agency Name and Address
U.S. Department of Transportation
Federal Railroad Administration
Office of Research and Development
Washington, D.C. 20590

13. Type of Report and Period Covered
Final Report
October 1985-June 1986

14. Sponsoring Agency Code
RRS-31

15. Supplementary Notes
*Under contract to: U.S. Department of Transportation
Research and Special Programs Administration
Transportation Systems Center
Cambridge, MA 02142

16. Abstract

Motivated by the occurrence of a long-running rail web fracture in service, dynamic fracture mechanics research was undertaken to (1) quantify the crack driving force due to the residual stresses induced by roller straightening operations, (2) determine dynamic fracture toughness values for rail steel, and (3) assess current analysis procedures for calculating dynamic fracture propagation in rail. As a first step, elastodynamic finite element analyses were made of full-section rail impact experiments conducted in Japan. These analyses revealed that the fracture propagation event in these experiments has an unexpectedly complex character. This behavior complicates the use of the raw crack jump length to measure the ability of the combination of a given rail steel and straightening operation to resist catastrophic fracture. Further analyses using a beam-on-elastic foundation model of a split rail provided a relation between the rail web residual stresses and the crack driving force. This relation indicates that, if the residual stresses in the failed rail were comparable to those reported in the literature, a long-running fracture could be driven by residual stresses alone. It was concluded from this preliminary work that a near balance can exist between the crack driving forces arising from the residual stresses induced by conventional straightening procedures and the dynamic fracture toughness values of some rail steels. Consequently, a major safety issue possibly exists that may require the development of screening procedures to assure the selection of fracture-safe rail for service. Recommendations are presented for continuing the research to verify the conclusions of this report and, if warranted, to develop the technical basis for a simple but reliable screening test.

17. Key Words	18. Distribution Statement
Rail, Fracture Mechanics, Residual Stress, Finite Element Analysis, Crack Arrest, Fracture Toughness, Full-Section Impact Test, Beam-On-Elastic Foundation Model	DOCUMENT IS AVAILABLE TO THE PUBLIC THROUGH THE NATIONAL TECHNICAL INFORMATION SERVICE, SPRINGFIELD, VIRGINIA 22161

19. Security Classif. (of this report)	20. Security Classif. (of this page)	21. No. of Pages	22. Price
unclassified	unclassified		

PREFACE

The Department of Transportation's Federal Railroad Administration (FRA) has an orgoing commitment for improving railroad safety. The safety of the track network is of prime importance in this goal. FRA's Office of Research and Development sponsored this study of the dynamic fracture toughness of steel track. The Transportation Systems Center (TSC) supervised the project under a contract to the Southwest Research Institute, Engineering and Materials Sciences Division.

S.G. Sampath, James Morris and Oscar Orringer of TSC were in close contact with the authors throughout this project. Background discussions were held with Roger Steele of the Association of American Railroads; Professor G.T. Hahn of Vanderbilt University; Professor C.H. Popelar of the Ohio State University; and Professor A. McEvily of the University of Connecticut. The authors are also highly appreciative of the results so kindly provided by Itaru Watanabe and Takao Gino, Nippon Kokan K.K. Technical Research Center, Kawasaki, Japan; and by Richard Rice of Battelle's Columbus Laboratories.

METRIC CONVERSION FACTORS

Approximate Conversions to Metric Measures

Symbol	When You Know	Multiply by	To Find	Symbol
LENGTH				
in	inches	*2.5	centimeters	cm
ft	feet	30	centimeters	cm
yd	yards	0.9	meters	m
mi	miles	1.6	kilometers	km
AREA				
in^2	square inches	6.5	square centimeters	cm^2
ft^2	square feet	0.09	square meters	m^2
yd^2	square yards	0.8	square meters	m^2
mi^2	square miles	2.6	square kilometers	km^2
	acres	0.4	hectares	ha
MASS (weight)				
oz	ounces	28	grams	g
lb	pounds	0.45	kilograms	kg
	short tons (2000 lb)	0.9	tonnes	t
VOLUME				
tsp	teaspoons	5	milliliters	ml
Tbsp	tablespoons	15	milliliters	ml
fl oz	fluid ounces	30	milliliters	ml
c	cups	0.24	liters	l
pt	pints	0.47	liters	l
qt	quarts	0.95	liters	l
gal	gallons	3.8	liters	l
ft^3	cubic feet	0.03	cubic meters	m^3
yd^3	cubic yards	0.76	cubic meters	m^3
TEMPERATURE (exact)				
°F	Fahrenheit temperature	5/9 (after subtracting 32)	Celsius temperature	°C

*1 in. = 2.54 cm (exactly). For other exact conversions and more detail tables see NBS Misc. Publ. 286, Units of Weight and Measures. Price $2.25 SD Catalog No. C13 10 286.

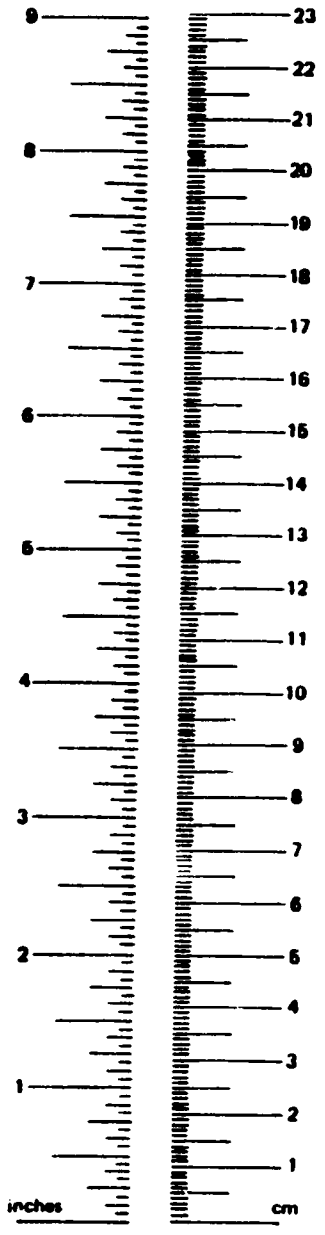

Approximate Conversions from Metric Measures

Symbol	When You Know	Multiply by	To Find	Symbol
LENGTH				
mm	millimeters	0.04	inches	in
cm	centimeters	0.4	inches	in
m	meters	3.3	feet	ft
m	meters	1.1	yards	yd
km	kilometers	0.6	miles	mi
AREA				
cm^2	square centimeters	0.16	square inches	in^2
m^2	square meters	1.2	square yards	yd^2
km^2	square kilometers	0.4	square miles	mi^2
ha	hectares (10,000 m^2)	2.5	acres	
MASS (weight)				
g	grams	0.035	ounces	oz
kg	kilograms	2.2	pounds	lb
t	tonnes (1000 kg)	1.1	short tons	
VOLUME				
ml	milliliters	0.03	fluid ounces	fl oz
l	liters	2.1	pints	pt
l	liters	1.06	quarts	qt
l	liters	0.26	gallons	gal
m^3	cubic meters	36	cubic feet	ft^3
m^3	cubic meters	1.3	cubic yards	yd^3
TEMPERATURE (exact)				
°C	Celsius temperature	9/5 (then add 32)	Fahrenheit temperature	°F

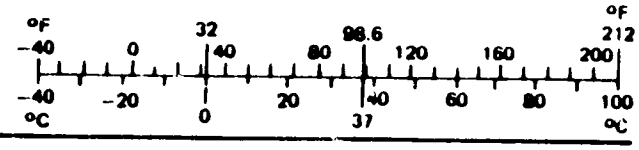

TABLE OF CONTENTS

LIST OF FIGURES

LIST OF FIGURES (continued)

LIST OF TABLES

EXECUTIVE SUMMARY

Elastodynamic finite element fracture mechanics analyses were performed to elucidate the conditions under which a long-running rail web fracture can occur. First, an analysis simulated an instrumented full-section rail impact fracture experiment on a conventional alloy rail conducted by Nippon Kokan K.K. (NKKK) in Japan. A second analysis used the dynamic toughness values that were deduced to predict crack propagation and arrest in another NKKK experiment. Because reliable residual stress states for the NKKK specimens were not available, an accurate prediction of the final arrested crack length was precluded. The effects of postulated residual stress states were nevertheless found to give good qualitative agreement with other NKKK experimental observations. In particular, it was found that compressive longitudinal web residual stresses promote long running straight cracks while tensile longitudinal web residual stresses lead to crack curving and arrest.

Of most significance, the finite element analyses revealed that a full-section impact test has an unexpectedly complex character. It appears that the total crack length results from a segment of rapid dynamic crack propagation that is followed by sequential quasi-static run/pause events. The initial dynamic portion of crack propagation can be reasonably well predicted by elastodynamic analysis procedures provided a residual stress dependent dynamic fracture toughness property is used. However, the synergism of the impact load and the residual stresses in the rail web that dominates the quasi-static cracking regime cannot be accomodated at present.

Because of the key role played by residual stresses in promoting unstable web fracture, further work employing a simple beam-on-elastic foundation model of a longitudinally split rail was performed. The model relates K_R, the stress intensity factor due to residual stresses, to σ_R, the compressive longitudinal web residual stress. This key result is

$$K_R = \frac{\sigma_R}{c}\left(\frac{pI}{2b}\right)^{\frac{1}{2}}$$

where b, c and I respectively are the web thickness, the distance from the crack plane to the centroid of the half rail, and the moment of inertia of the half rail, while p is a constraint factor that equals 1 for track and 2 for a full-section impact test. Using a typical value of σ_R = 150 MPa obtained from the literature and standard rail dimensions, this relation gives K_R = 24 MPam$^{\frac{1}{2}}$ for track. This estimate can be compared with crack arrest toughness (K_{Ia}) values: for standard rail steel K_{Ia} = 29 MPam$^{\frac{1}{2}}$, and for premium alloy rail K_{Ia} = 17 MPam$^{\frac{1}{2}}$. Because rapid crack propagation in track is not likely if $K_{Ia} > K_R$, this analysis is therefore consistent with the absence of long-running dynamic crack propagation events in standard rail and with the actual occurrence of such an event in a premium alloy rail.

The findings of this research indicate that, if the rail does not have adequate dynamic fracture resistance, rail residual stresses can give rise to crack driving forces that are sufficient to maintain a long-running web fracture. Consequently, the accurate determination of both rail steel dynamic structure toughnesses and residual stresses are important for rail safety. It is concluded that instrumented full-section impact tests that are interpreted by dynamic fracture mechanics procedures are needed to determine rail properties that will preclude long-running fracture events in track.

1. INTRODUCTION

As described by Orringer and Tong [1], a train derailment near Marshall, Texas, on 12 November 1983 resulted from catastrophic crack propagation in the web of a rail. The fractured rail was a roller straightened "premium-alloy" steel. The combination of a crack initiation site at the rail end caused by torch cutting in a repair operation, high tensile residual stresses in the rail head, and the lower fracture toughness of premium alloy steel is thought to have created a near-critical fracture condition. Evidently, rapid unstable crack propagation was then triggered by the added dynamic stresses induced by the fast moving train striking a 3/16-inch high rail misalignment. The reconstructed rail showing the multiple branches that fragmented a 10 meter length of rail, taken from John et al [2], is shown in Figure 1.

Owing to their improved wear resistance and other superior attributes, there is an economic incentive to make wider use of premium alloy steels in track service. Indeed, a sizable amount of this rail has been purchased and is currently in inventory. However, in view of the derailment triggered by the event shown in Figure 1, together with other incidents that have occurred with premium-alloy steel [1], the railroad industry must be concerned with the possible inordinate susceptibility of these steels to catastrophic fracture. On the basis that crack initiation cannot be absolutely precluded (e.g., because of fatigue cracks), the dynamic plane strain crack arrest toughness K_{Ia} becomes a key rail steel property in a safety assessment.

This research was initiated to learn if dynamic fracture mechanics techniques can be extended to determine and apply K_{Ia} values in track applications. In the technical approach envisioned, an assessment was to be made of a general procedure that has been effectively used for crack arrest assessments in many other engineering problems. First, elastodynamic finite element analyses were to be made of an instrumented rail fracture experiment to infer the speed-dependent dynamic fracture toughness property, K_{ID}. These data were then to be used to predict crack propagation and arrest for that rail steel in different loading conditions. Comparison of further experimental results would provide a critical check on the validity of the approach. In addition, because the K_{ID} property contains the conventional K_{Ia} property as its zero crack speed limiting value, and K_{Ia} is in turn generally related to K_{Ic}, these data would also be assessed by comparison to open literature data.

Confounding the analysis problem for rail steels are (1) the presence of (generally unknown) residual stresses, (2) the lack of a basis for a sound two-dimensional analysis model for a rail, and (3) the paucity of crack run/arrest data on rails that would provide the boundary conditions for an analysis model. Therefore, this research was undertaken in a heuristic spirit with straightforward assumptions and approximations being introduced to overcome the first two of these difficulties. The third difficulty vanished when it was coincidentally learned that crack length and crack opening displacement histories in full-section impact tests on rails, conducted by the Nippon Kokan K.K. (NKKK) Steel Company of Japan, were available [3]. Detailed sample data provided by Watanabe and Gino [4] made it possible to undertake this study.

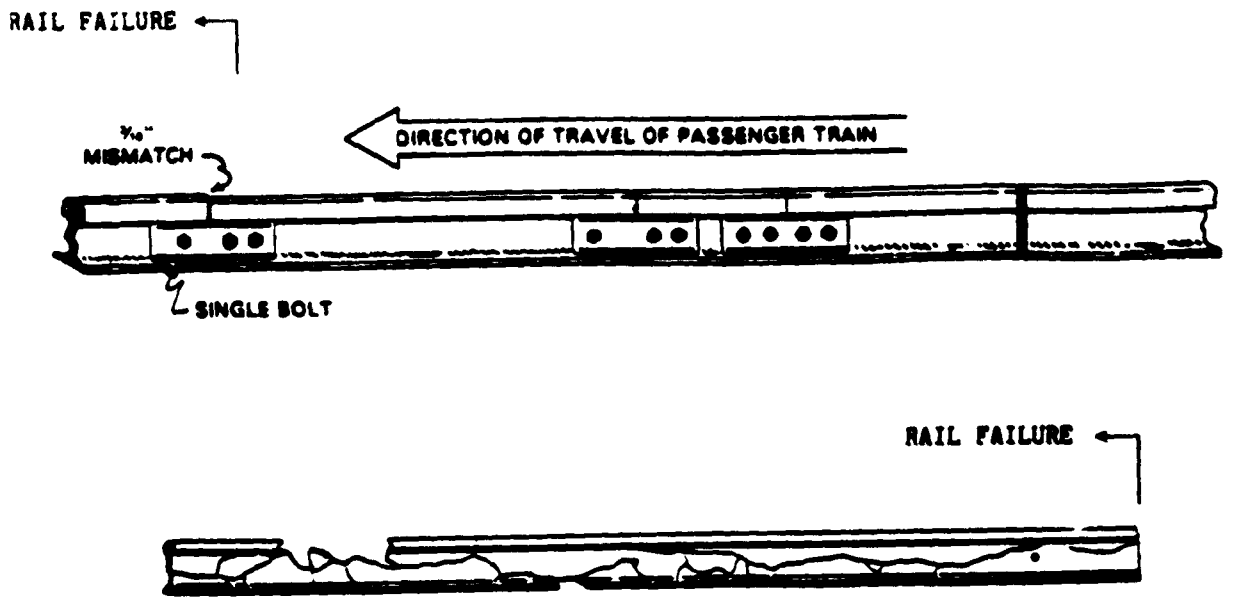

Figure 1. Reconstructed Rail Involved in a Dynamic Fracture Event [2].

2. TECHNICAL BACKGROUND FOR THE APPLICATION OF DYNAMIC FRACTURE MECHANICS TO RAIL STEELS

This report describes the analyses that were performed to extract dynamic fracture toughness values of standard rail steels from the NKKK full-section impact experiments on these steels. The technology that underlies the analyses conducted in this project is that of dynamic fracture mechanics. Because of its direct bearing on the work that was conducted, an appreciation of the subject is necessary for an understanding of the technical approach that has been employed. Accordingly, a brief review of the subject is provided in this section along with capsulations of the Nippon Kokan full-section impact test results and of the pre-existing rail steel fracture toughness and residual stress data bases.

Readers already familiar with the status of this technology may prefer to omit this background review and to proceed directly to the description of the technical accomplishments of the program that begin in Section 3 of this report.

The background discussion is followed by a description of the technical effort that was performed. This is reported in Sections 3 and 4 with discussions and conclusions given in Section 5. Recommendations on the further research that is needed to complete the research and thereby provide the basis for rail safety assessment procedures are offered in Section 6.

2.1 Basis of Elastodynamic Fracture Mechanics

Two apparently different points of view exist for the arrest of a rapidly propagating crack [5]. One is that crack arrest can be considered as the reverse in time of crack initiation. This implies the existence of a material constant for crack arrest that is numerically equal to the static value of the crack driving force that corresponds to the crack length at the arrest point. An alternative point of view is one based upon a dynamic equality that governs the moving crack. Crack propagation occurs in this more general approach so long as the crack driving force is numerically equal to the resistance presented by the material to crack advance. Crack arrest occurs when the equality is no longer satisfied. Because the focal point is the crack growth process, this is known as the "kinetic" approach.

Because dynamic effects generally exist at crack arrest, in principle, the static approach is an oversimplification. Care must therefore always be taken in using arrest toughness data extracted from small-scale test specimens; particularly the DCB specimen. In contrast, in most practical applications, crack arrest occurs prior to the return of reflected stress waves to the crack tip whereupon the static and the kinetic approach are indistinguishable. However, there are at least two practical problems where this is not so: a gas transmission pipeline and a rail. Before reviewing the former (see Section 2.3), the necessity of a kinetic approach for application to rails can be readily assessed, as follows.

At the commencement of rapid crack propagation, compressive stress waves are always radiated outwards from the crack tip. These waves will reflect from the free surfaces that parallel the crack plane (e.g., the upper surface of the rail head) as tensile waves and will return to the crack plane to enhance the crack driving force. The maximum amount of crack advance that can occur before the reflected stress waves begin to interact with the crack tip is then given by the simple relation

$$(\Delta a)_{max} = 2h \frac{\bar{V}}{C_1} \tag{1}$$

where h is the distance between the crack plane and the nearest parallel free boundary of the component, $\bar{V}$ is the average crack speed, and C_1 is the highest elastic wave speed. Taking h = 85 mm and $\bar{V}/C_1 = 0.2$, Equation (1) suggests that $(\Delta a)_{max}$ would be about 34 mm for a rail web. It is therefore clear that the analysis of crack propagation in a rail web that approaches the conditions corresponding to Figure 1 requires a kinetic approach.

Rapid crack propagation can be considered to occur in the kinetic point of view under the condition that the dynamically computed crack driving force is numerically equal to the material's resistance to crack extension. Within the confines of elastodynamic behavior, this is expressed as

$$K = K_{ID}(V,T) \tag{2}$$

where K_{ID}, the dynamic fracture toughness*, is a function of the instantaneous crack speed V and the temperature T. In Equation (2), K is the dynamically calculated value of the stress intensity factor. Therefore, K generally must be determined as part of the solution of an elastodynamic initial value, moving boundary value problem.

In the kinetic approach, arrest occurs at the position and time for which K becomes less than the minimum value of K_{ID}, and remains less, for all greater times. Within this framework, the arrest criterion is the inequality

$$K < K_{IA}(T) \tag{3}$$

where $K_{IA} = K_{ID}(0, T)$ denotes the minimum value of K_{ID} with respect to crack speed. It is important to note that K_{Ia}, the static crack arrest toughness, will be a good approximation to the true crack arrest toughness K_{IA} provided that arrest is achieved in the absence of reflected stress waves in the material characterization test used to measure K_{Ia}.

---

* It will be considered in this work that the lateral constraint attending a propagating through-wall crack in the web of a rail corresponds to a plane strain condition. Accordingly, the linear elastic fracture initiation, propagation, and arrest properties will be designated as K_{Ic}, K_{ID}, and K_{Ia}, respectively. The justification for the plane strain assumption is given in Section 2.5 of this report.

2.2 Dynamic Fracture Toughness Correlations

The K_{ID} measurements that have so far been made for metals and polymers all have the same qualitative form [5]. It has been found that they can all be correlated by an empirical relation having the form

$$K_{ID} = \frac{K_{IA}}{1-(\frac{V}{V_\ell})^m} \tag{4}$$

where K_{IA}, V_ℓ and m are empirical temperature-dependent material constants. While it is not imperative to use Equation (4) as a curve fitting device, it may be of interest to recognize that these constants have a clear physical interpretation. Specifically, V_ℓ corresponds to a limiting crack speed, K_{IA} corresponds to the nearly constant value in the low crack speed regime, while m is a dimensionless parameter that dictates the shape of the curve.

It might be recognized that V_ℓ is not generally associated with an elastic wave speed. In fact, it is typically lower than the longitudinal wave speed C_1 by approximately a factor of five. For example, for Type 4340 steel, $V_\ell \doteq 1200$ m/s at room temperature, while $C_1 \doteq 6000$ m/s. Thus, $V_\ell/C_1 \doteq 0.2$. Similar results are obtained for most materials; see Reference [5].

Of some significance for characterizing crack arrest, results of the type representable by Equation (4) provide a pragmatic basis for the use of the static arrest toughness. The basis is that, provided a K_{Ia} value is obtained under the proper conditions (i.e., a short crack jump), it will be a good approximation to K_{IA}. It is of key importance in the general approach to be followed in this research to recognize that valid K_{Ia} data can contribute to the K_{ID} data base for the analysis of crack propagation and arrest in rails. This is true even in applications where reflected stress waves do play a role. Of course, dynamic analyses must then be used to determine K.

A procedure that has been found to be effective for generating K_{ID} data is a hybrid experimental/computational procedure known as a "generation-phase" analysis. In this procedure, experimental data in the form of crack lengths and load point displacements, both as functions of time, are used as the inputs to an elastodynamic finite element model of the geometry used in the experiments. These data then allow an initial value, moving boundary value problem to be solved. This determines the dynamic stress intensity factor as a function of time. Then, by postulating that Equation (2) is valid, K_{ID} values for the material as a function of the instantaneous crack speed and test temperature can be inferred from the calculated K values.

The counterpart of a generation-phase analysis is known as an "application-phase" analysis. This requires K_{ID} data to be available at the outset. Then, for specified initial and boundary conditions, a prediction of crack length versus time (including crack arrest, if it occurs) can be obtained using Equation (2) with, for example, the prescribed K_{ID} data in the form of Equation (4). Both generation-phase and application-phase analyses are performed in the research described in the following sections.

A simplified version of Equation (4) has often been found to be useful in constructing a K_{ID} relation. This is

$$K_{ID} = K_{Ia} + DV^m \tag{5}$$

which has been derived from Equation (4) by assuming that $K_{IA} = K_{Ia}$, and that $V << V_a$. The virtue of Equation (5) is that, if K_{Ia} data exist, they can be used along with a minimum of propagation data to develop a K_{ID} relation. In fact, this relation plays a key role in the work reported herein. Specifically, by utilizing estimates of K_{Ia} for rail steels, experiments in which dynamic crack arrest does not occur can be analyzed to determine the parameters D and m; see Section 3.

2.3 Assessments of Dynamic Fracture Mechanics Analysis Procedures

Currently, K_{ID} results are entirely empirical. They nevertheless provide a basis for attacking practical problems. With estimates for the maximum anticipated K for service conditions and K_{ID} data for candidate materials, the use of Inequality (3) permits material qualifications to be established that will preclude catastrophic fracture. This approach has been effectively employed for nuclear pressure vessels, cryogenic storage tanks and gas transmission pipelines [6]. In anticipation that these will display some key elements in common with rail web fracture, the crack driving forces for a long-running axial crack in a pressurized pipeline in two sets of operating conditions are shown in Figure 2. Comparisons of crack speeds derived from these curves with full-scale experimental results are given in Figure 3. These results are taken from References [7, 8].

By the use of steady-state crack propagation conditions, the crack driving force (expressed in Figure 2 in energy release rate terms) for a gas transmission pipeline was evaluated as a function of crack speed. Of particular importance is the existence of a maximum crack driving force that can be quantitatively determined by this procedure--see Figure 2. Knowing this maximum value allows a minimum fracture toughness value to be specified. Specifically, using $K^2 = EG$, a maximum K can be determined from a result such as shown in Figure 2. This provides a quantitative measure of the necessary toughness level that would preclude a steady-state condition. Use of a material with that toughness assumes that, even if unstable crack propagation commences, a long-running fracture should not be possible.

Work of Kalthoff et al [9] showed that dynamic fracture toughnesses could be obtained by optical methods that compared well with those computed in conventional ways. More recently, jointly conducted research at the Southwest Research Institute and the California Institute of Technology has been initiated to critically examine the uniqueness of the K_{ID} property [10]. This is being done by simultaneously obtaining results on 4340 steel by the method of caustics in reflection and by using the generation-phase analysis approach described above in which experimentation is combined with finite element analysis to obtain K_{ID} values.

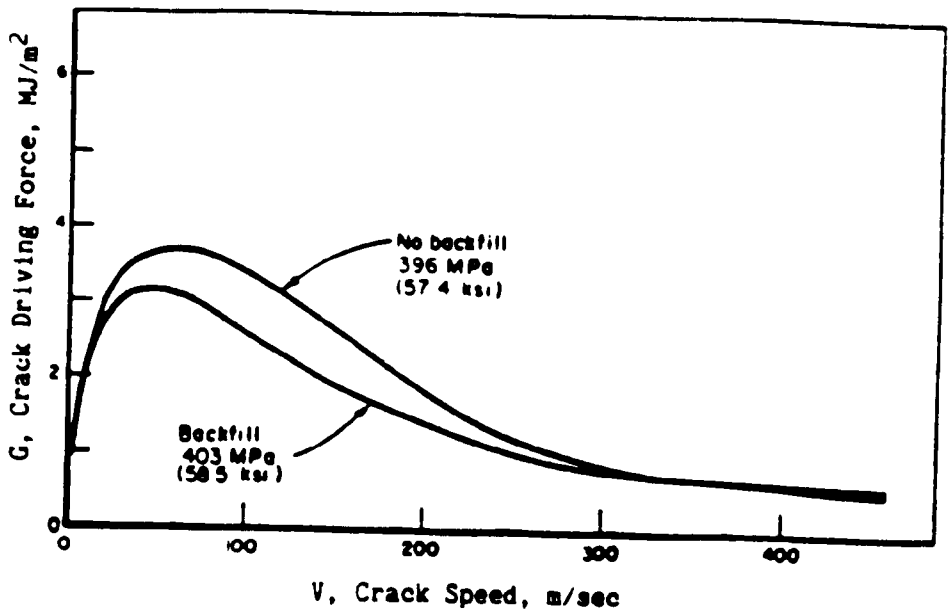

(a) Pipe diameter = 26 inches, wall thickness = 0.31 inches, line pressure = 1100 psi.

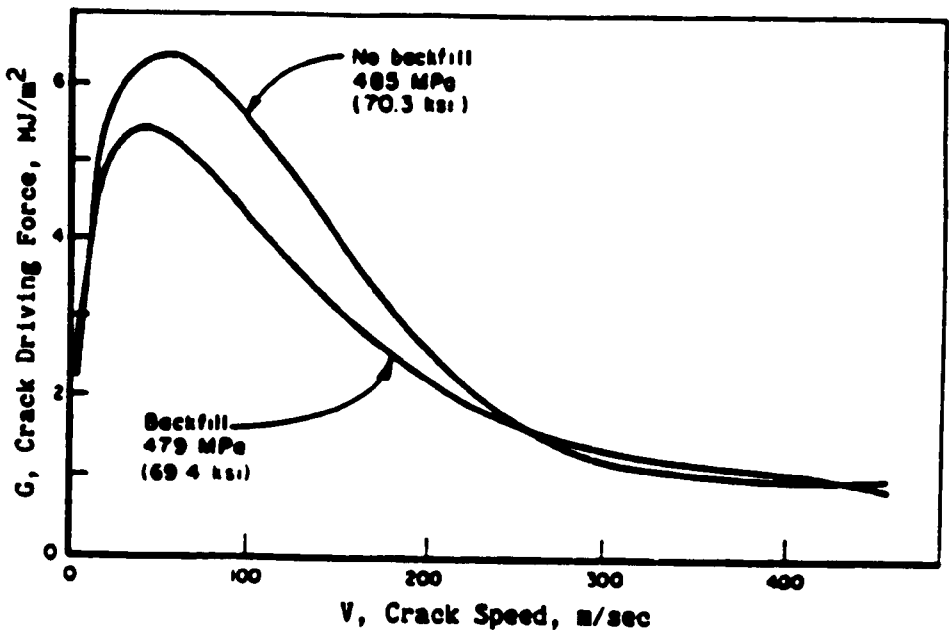

(b) Pipe diameter = 36 inches, wall thickness = 0.33 inches, line pressure = 1100 psi.

Figure 2. Theoretical Crack Driving Force Values for Steady State Crack Propagation in Gas Transmission Pipelines.

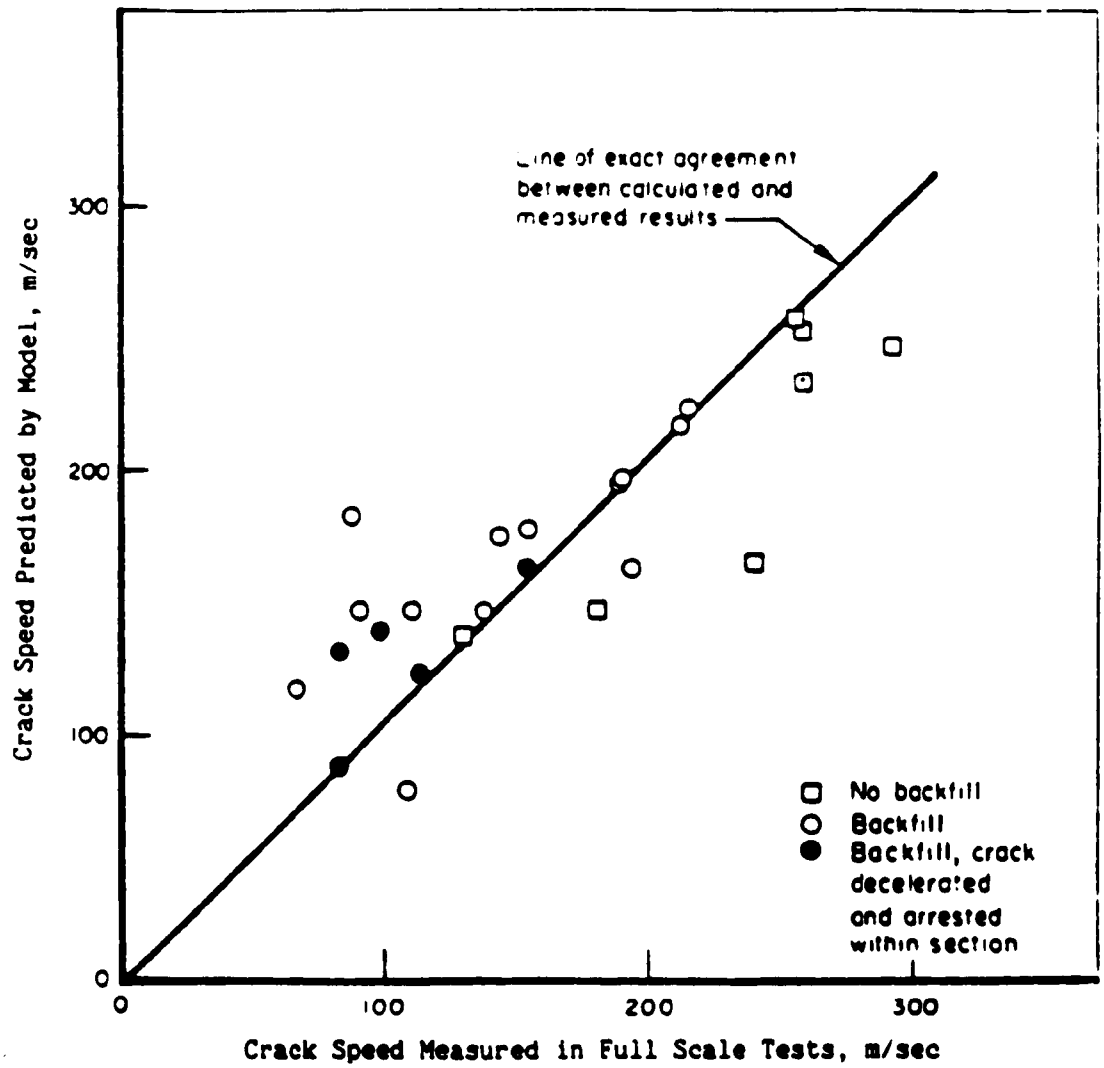

Figure 3. Comparison of Predicted Crack Speeds in a Gas Transmission Pipeline with Full-Scale Pipe Fracture Propagation Experimental Data

Preliminary results of the SwRI and Cal Tech techniques are in good qualitative agreement. This finding indicates that the kinetic approach is fundamentally sound although some difficulties in current procedures for extracting the K_{ID} property--particularly in load-point-driven fracture propagation experiments in specimens where stress wave reflections play a prominent role--are also being revealed by these results. While clearly demonstrating the necessity for great care in the experimentation, this comparison nevertheless provides strong support for the use of this technique for rails.

2.4 NKKK Fracture Propagation Test Procedures and Results

Because research that advances the applicability of the subject must blend computations with experimentation, this research has been possible because of the experimental work performed by Watanabe and Gino of the Nippon Kokan K.K. (NKKK) Technical Research Center [3,4]. Their experiments were patterned after the full-section impact test procedure apparently first employed by Steele of the Association of American Railroads (AAR). As evident in Figure 4, the full section impact test is conducted on a horizontal rail with an initial crack oriented to favor propagation along the mid plane of the rail web. Unstable crack propagation is initiated by dropping a weight on a wedge placed in a split pin that is located in a circular hole in the rail web. A blunt crack emanating from the hole is employed to direct the crack along the rail web. Details of the split pin loading device used in that test are provided in Figure 5.

In the NKKK work, full-section impact tests were performed at different temperatures and drop heights, thus varying the extent and speed of the unstable crack propagation events that were observed. A major distinction in the results for different steels was in the degree of crack path curving that was evident. In most of their experiments, the crack invariably turned to the rail base and did so, often abruptly, within a relatively short distance. While crack curving is clearly an important aspect of the general problem, to initiate this work in a relatively straight forward manner, attention was confined to the NKKK experiments in which the cracks propagated in a relatively straight line; i.e., the experiments performed on the steel designated by NKKK as STDC. Figure 6 shows the crack paths obtained for two tests on the STDC steel and, for contrast, a test on their AHH steel.

Tables 1 and 2, using data taken from References [2] and [3], display the chemical compositions and the mechanical properties of various rail steels including those contrasted in Figure 6. It can be seen from these data that the STDC steel, both in chemical composition and in its mechanical properties, is close to the standard rail steel. Of most significance to this research, the NKKK work included measurements of the crack length and crack opening displacement histories. Figure 7 shows the locations of the strain gages used to dynamically determine the crack tip position as a function of time for the two materials of interest here. The discrete data corresponding to two of the experiments shown in Figure 6, obtained from Watanabe and Gino [4], are given in Table 3 with the dynamic crack opening displacements shown in Figure 8. As may be clear from the background discussion given in the preceding, it is the absence of these data in the AAR experiments that precludes their analysis and, accordingly, necessitates exclusive consideration of the NKKK experiments here.

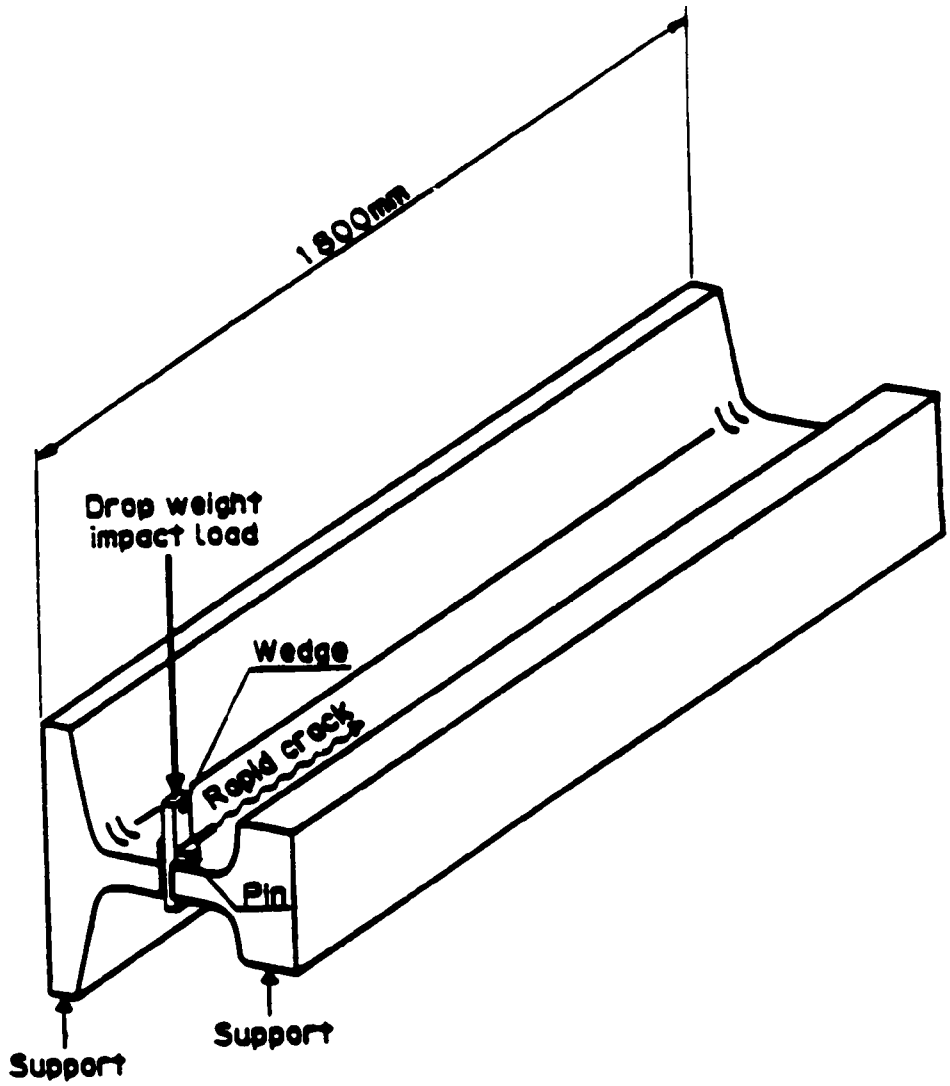

Figure 4. Schematic Illustration of NKKK Full Section Impact Test Procedure for Rail Fracture Propagation Experiments

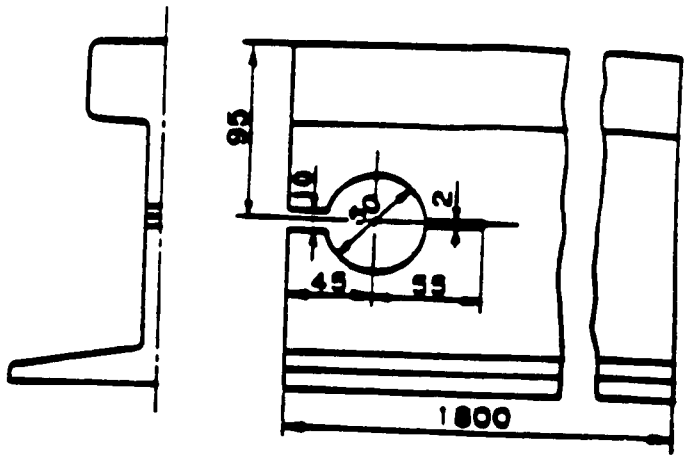

(a) Specimen Geometry

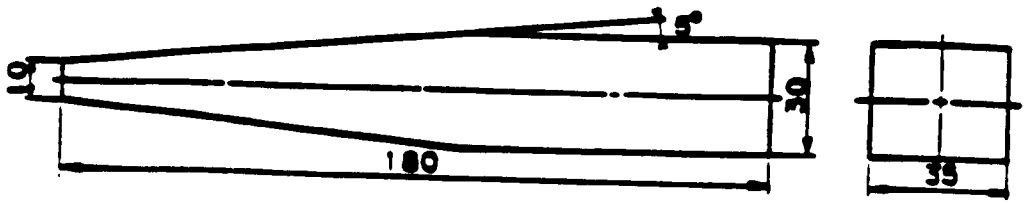

(b) Wedge Geometry

Figure 5. Details of NKKK Full-Section Impact Test Loading Device (all dimensions in mm)

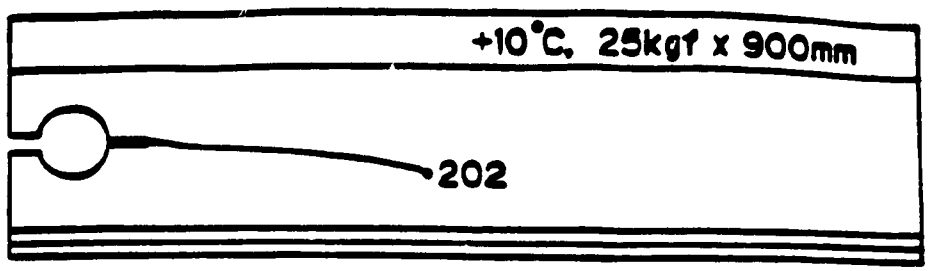

(a) STDC Steel -- 900 mm Drop Height

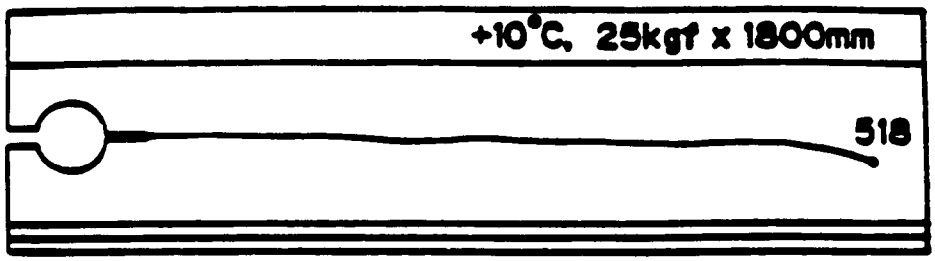

(b) STDC Steel -- 1800 mm Drop Height

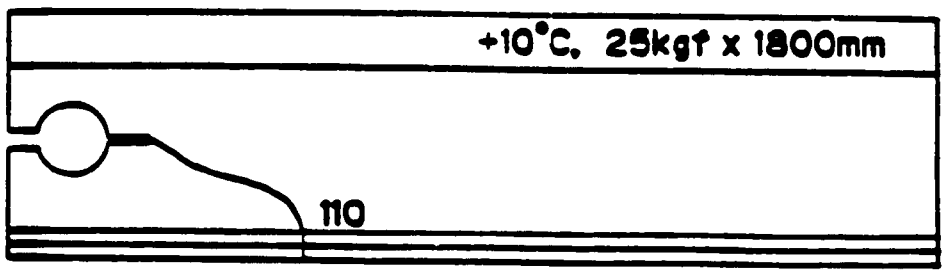

(c) AHH Steel -- 1800 mm Drop Height

Figure 6. Crack Paths Observed in Three NKKK Full-Section Impact Tests Conducted at 10°C with 25 kg Drop Weights (numbers at end of crack denote total crack length at arrest in mm).

Table 1. Comparison of Chemical Composition and Heat Treatment in Selected Rail Steels

Steel	Heat Treatment	Chemical Composition (wt %) C	Si	Mn	Cr	V
		NKKK Rail Steels [3]				
STDC	as rolled	0.78	0.23	0.93	-	-
AHH	slack quench	0.77	0.56	0.85	0.44	.059
		Reference Rail Steels [2]				
Standard		0.80	0.20	0.90	-	-
Failed Rail		0.79	0.19	1.12	0.87	.06

Table 2. Comparison of Mechanical Properties of Web in Selected Rail Steels

Property	NKKK Rail Steels [3] STDC	AHH	Reference Rail Steels [2] Standard	Failed Rail
Yield strength (MPa)	509	651	510	765
Tensile strength (MPa)	914	1080	917	1200
Elongation (%)	10.0	10.8	11.0	8.3
Reduction of area (%)	15.9	12.0	18.0	9.2
Absorbed energy at 20°C (ft lbs)	2.9	3.4	3.9	1.5

Table 3. Crack Length Histories Measured in NKKK Full-Section Impact Tests [4]

Temperature: 10°C
Drop Weight: 25 kg
Drop Height: 1800 mm

STDC rail steel		AHH rail steel	
distance from notch tip (mm)	time[a] (μ sec)	distance from notch tip (mm)	time[a] (μ sec)
5	334	5	400
20	362	15	426
50	418	30	450
80	485	45	480
110	968	60	512
140	1184	75	563
170	1902	90	733
200	2336	105	--
518[b]	--	110[b]	--

(a) These values are as reported by NKKK and are relative to their trigger time. Crack initiation has been estimated in this report to occur at 324 μsec after the trigger. Consequently, times from initiation can be obtained from the NKKK data by subtracting 324 μsec; cf, Figure 17.

(b) Observed arrest point--time of arrest not available.

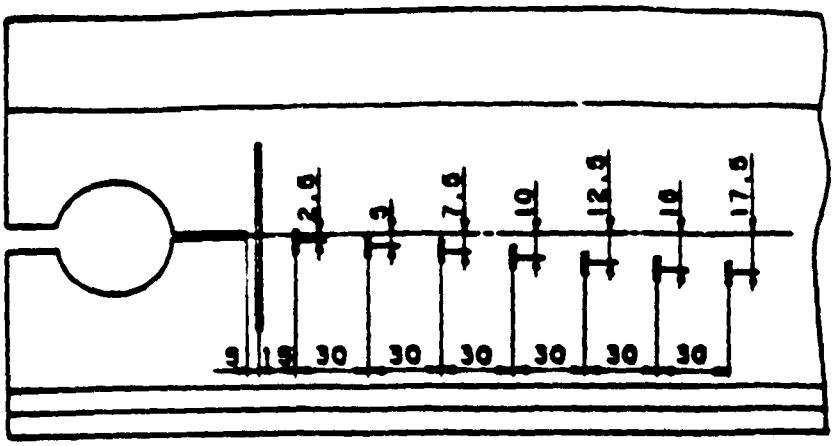

(a) STDC Rail Steel

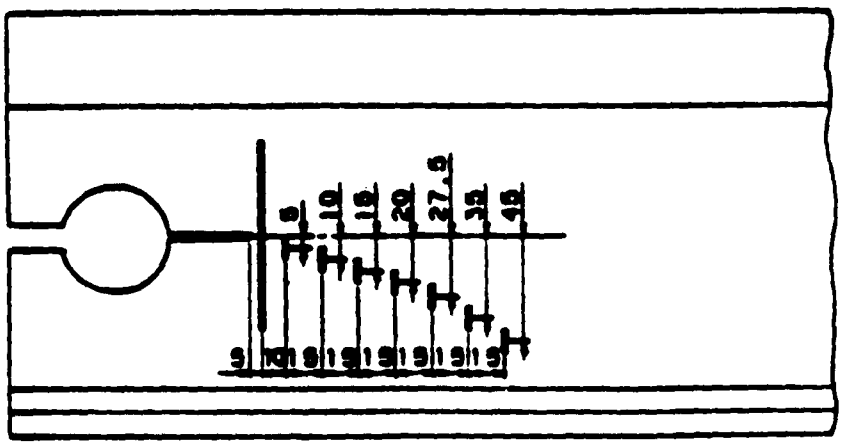

(b) AHH Rail Steel

Figure 7. Location of Crack Propagation Gages in NKKK Full-Section Impact Tests

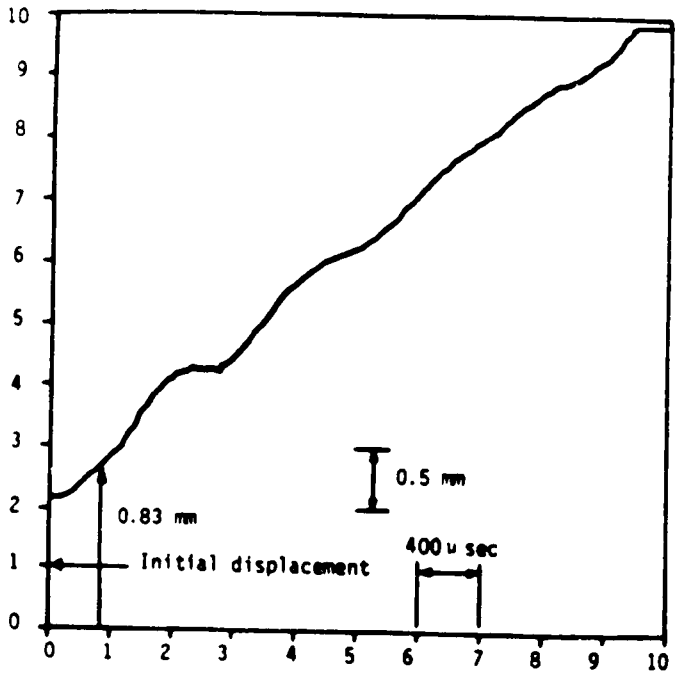

(a) STDC Rail Steel

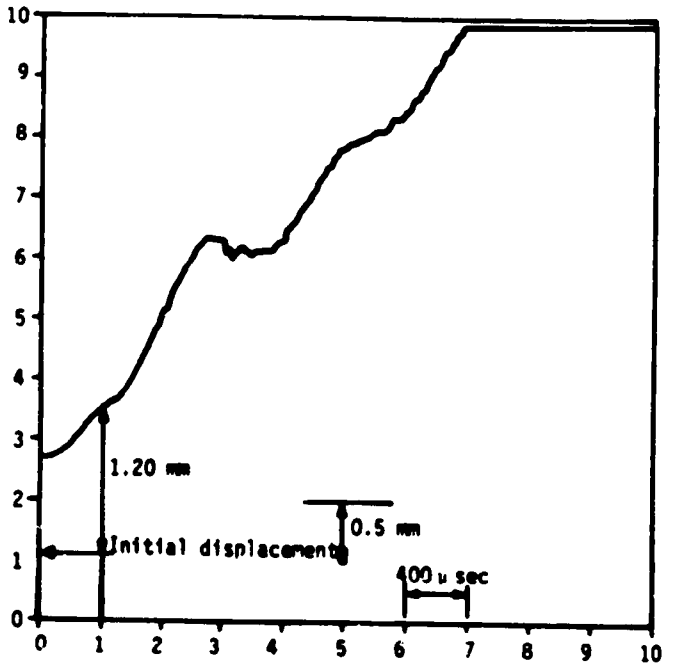

(b) AHH Rail Steel

Figure 8. Crack Opening Displacement Histories Obtained in NKKK Full-Section Impact Tests at 10°C, 25 kg Drop Weight, and 1800 mm Drop Heights.

2.5 Available Rail Steel Fracture Toughness and Residual Stress Data

As discussed in the above, the critical material property in a crack propagation/arrest assessment is K_{Ia}, the plane strain crack arrest toughness. While unequivocal values of K_{Ia} do not currently exist for rail steels, various possible estimation procedures can be used to infer representative values. In particular, although differing numerically from the initiation toughness, arrest toughness values are generally comparable to, and can be estimated from, dynamic initiation values. For example, an empirical relation developed for bridge steels relates K_{Id}, the dynamic initiation toughness, to the Charpy energy by

$$K_{Id} = [5EC_v]^{\frac{1}{2}} \tag{6}$$

where E is the elastic modulus (psi) and C_v is the Charpy energy (ft lbs). This relation gives K_{Id} in units of psi-in$^{\frac{1}{2}}$.

A result such as given by Equation (6) can be connected with K_{Ia} as follows. Below the transition temperature (typically about 140°C for rail), K_{Ia} is approximately equal to the lower limit of K_{Id} with increasing loading rates. Assuming this to be true here, the C_v values given in Table 2 can be used with Equation (6) to estimate K_{Ia} for rail steels. Hence, a possible estimate is given by

$$K_{Ia} = .0011\ [5EC_v]^{\frac{1}{2}} \tag{7}$$

where the introduction of the multiplicative factor of .0011 gives K_{Id} in MPam$^{\frac{1}{2}}$ for E given in psi and C_v in ft lbs.

Using the values given in Table 2 and taking $E = 3\times10^7$ psi, the K_{Ia} values obtained from Equation (7) for the standard composition rail and for the failed rail, respectively, are 27 MPam$^{\frac{1}{2}}$ and 17 MPam$^{\frac{1}{2}}$. For the NKKK steels the K_{Ia} values so inferred would be 23 MPam$^{\frac{1}{2}}$ for the STDC material and 25 MPam$^{\frac{1}{2}}$ for the AHH material.

Tetelman and Stone [11] suggested that a good approximation for rail steels is given by $K_{Ic} = 1.4\ K_{Id}$ where K_{Ic} is the plane strain fracture toughness for initiation. Again, on the heuristic basis that $K_{Id} \doteq K_{Ia}$, it follows that K_{Ia} values for rail steel can be estimated from the alternative relation:

$$K_{Ia} = 0.7\ K_{Ic} \tag{8}$$

Supporting this estimate are results recently obtained by an ASTM committee working to develop a crack arrest standard. These show that the ratio K_{Ia}/K_{Ic} for A533B steel is approximately a constant very nearly equal to 2/3 over a wide range of temperatures.

In order to utilize Equation (8), a survey of K_{Ic} data published in the open literature was made. A significant degree of scatter was noted in the results reported in each investigation. Further recognizing that the rail steel compositions and other particulars may not be the same from one study to another, only the average of the results was taken. Table 4 provides these results. Using these results, it can be concluded from Equation (8) that K_{Ia} values for standard rail range from about 20 MPam$^{\frac{1}{2}}$ to 34 MPam$^{\frac{1}{2}}$. This is comparable to the value of 27 MPam$^{\frac{1}{2}}$ obtained from Equation (7). Because no more precise value can be obtained for the purposes of this report, the value of K_{Ia} = 29 MPam$^{\frac{1}{2}}$, obtained from Equation (8) using the average K_{Ic} value in Table 4, is taken as a reasonable estimate for standard rail steel.

The data displayed in Table 4 can also be used to examine the assumption of plane strain conditions. Specifically, the standard that governs fracture toughness testing, ASTM E-399, dictates that, for plane strain conditions to be valid, the plane strain plastic zone must be less than about one fiftieth of the specimen thickness. If the rail web thickness is denoted by b, the thickness at the crack tip permitting the plane strain assumption can be expressed as [5]

$$b > 2.5\left(\frac{K_{Ic}}{\sigma_Y}\right)^2 \tag{9}$$

where σ_Y denotes the yield stress. Now, Using the data in Tables 3 and 4, the right hand side of Inequality (9) for the materials of interest here range from 3.2 mm for the failed rail to 20 mm for standard rail steel. A typical value is b = 17 mm; cf, Figure 11(a). Hence, plane strain conditions are clearly valid for the failed rail. However, standard rail is marginal by this criterion. Nonetheless, because of the large conservatism embodied in Inequality (9), plane strain conditions are believed to be justifiable herein.

Of great importance in understanding the NKKK full-section impact test and, presumably, rail performance in general, are the residual stresses introduced by roller straightening operations. From the incidents cited for premium alloy rail by Orringer and Tong [1] and from other unpublicized incidents, it is clear that these rails include web tensile transverse residual stresses that assist in driving a crack longitudinally along the web. In other rails the residual stresses may be decisive in turning a crack to the flange; see Figure 6.

Anticipating that a synergistic effect exists between the residual stresses and the dynamic fracture toughness that determines the crack path and point of arrest, it is important to assimilate the residual stress data that exists for rail steels. Figures 9 and 10 illustrate the data that are available. Figure 9 shows results reported by the NKKK on AHH steel which feature tensile longitudinal residual stresses in the rail web [4]. These contrast with the results of Figure 10 for standard rail steel reported by the International Union of Railways Office for Research and Experiments (ORE) which show compressive web residual stresses [20]. Similar to the ORE results are the data of Rice [21]. The latter two sets of data will be drawn upon in Section 4.

Table 4. Average Room Temperature Fracture Initiation Toughness Values Obtained for Standard Rail Steel by Various Investigators

Investigators	K_{Ic} (MPam$^{\frac{1}{2}}$)
Jones and Rice [12]	36[a]
Park and Fletcher [13]	47
Kalousek et al [14]	40
Stone and Steel [15]	29
Marich and Curcio [16]	49
Barsom and Imhof [17]	42
Fowler and Tetelman [18]	43
McEvily and Ochi [19]	35
Average	41

(a) K_Q value

* For comparison with the values for standard rail provided in Table 4, Jones and Rice [12] report K_{Ic} = 29 MPam$^{\frac{1}{2}}$ for the failed rail. Using Equation (8), a value of K_{Ia} = 20 MPam$^{\frac{1}{2}}$ would then be obtained for this rail. This is reasonably close to the value K_{Ia} = 17 MPam$^{\frac{1}{2}}$ obtained from Equation (7); see discussion on page 17.

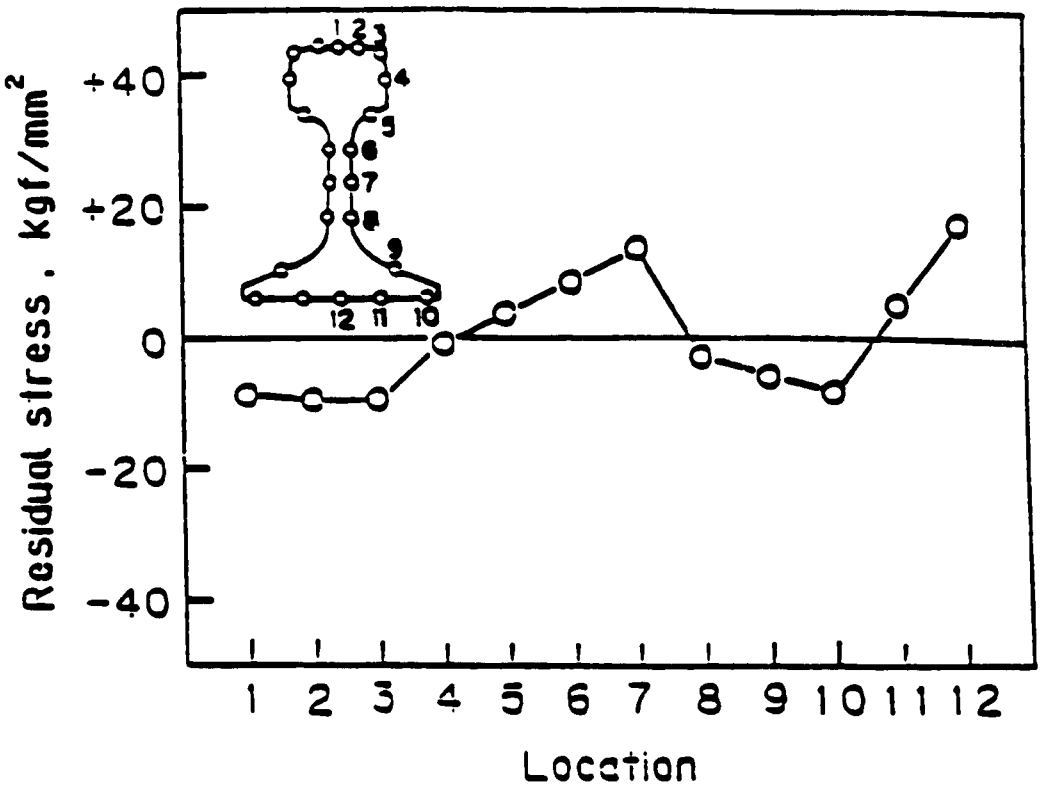

Figure 9. Longitudinal Direction Residual Stresses Determined by NKKK for the AHH Material [4].

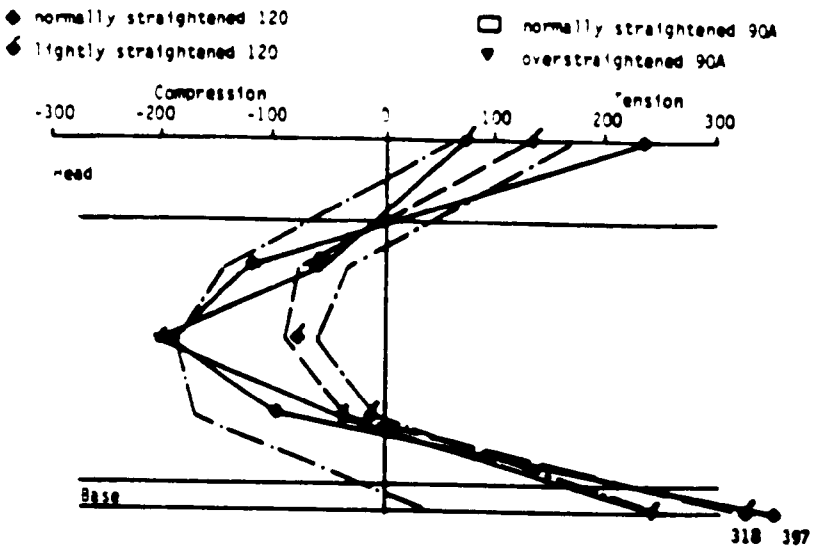

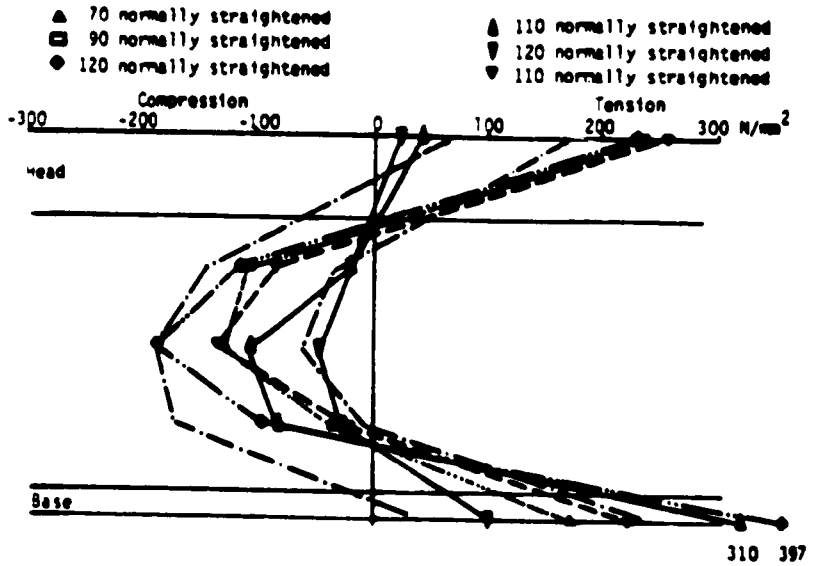

Figure 10. Longitudinal Direction Residual Stresses Determined on Standard Rail Steel by ORE [20].

3. FINITE ELEMENT FRACTURE/ARREST ANALYSES FOR RAIL STEEL

With the discussions given in the preceding section as a basis, the elastodynamic fracture mechanics finite element analyses of the NKKK rail fracture experiments are described in this section. These analyses initially ignored residual stresses. Consideration of the likely presence of residual stresses in the rail web was addressed in Section 3.5 et seq.

3.1 Finite Element Analysis Procedure

The elastodynamic finite element computer code SWIDAC used in this work solves the equations of motion using a displacement-based finite element formulation with quadratic isoparametric quadrilateral finite elements. It has been found that singular elements or other types of special crack tip elements are not necessary. Crack tip nodes are released using a linear force reduction over several time steps to model crack growth. This scheme, which allows both generation and application phase modeling, has been described in detail by Jung et al [22]. Time integration is performed using an implicit (Newmark-Beta) scheme. A time step of 1.0 μsec was used in the crack propagation analyses. The basis for the rail cross section dimensions selected for this study is given in Figure 11.

The dimensions of the rail cross section used in the NKKK experiments are shown in Figure 11(a). It is readily obvious that, even for a crack that propagates at the center of the web, a rail is nonsymmetric. Nevertheless, at this initial point in the research, a two-dimensional model was used that considered the crack to propagate along a longitudinal line of symmetry. This approximation, while obviously neglecting the geometric differences between the rail head and base, nevertheless maintains the mass and moment of inertia of the actual rail cross section; see Figures 11(b) and 11(c).

The rail geometry used in the computations reported herein is shown in Figure 11(b). A rail cross section that was used in preliminary analyses, Figure 11(c), was 20% less stiff than this. These gave results that did not differ significantly. This finding indicates that the analysis is not very sensitive to small changes in cross-section, provided the thickness at the crack plane is the same. This suggests that the symmetric idealization of the nonsymmetric cross section may not be inappropriate. The symmetric finite element model is shown in Figure 12.

The finite element model shown in Figure 12 consisted of 396 elements. The hole for the wedge was ignored on the basis of previous studies that have shown the effect of such holes to be inconsequential. In this study, the split collar that travels along with the rail as it displaces (see Figure 5) was also neglected. This omission roughly balanced the mass of the 17mm thick material that occupies the hole in the model.

An inertia enhanced version of the path-independent contour integral J is used by SWIDAC as the criterion for crack initiation under elastodynamic conditions [5]. The contour for the J-integral is shown in Figure 12. This contour shifts to the right by one element as each element is released. As a check, a smaller contour was also used. Consistent with results obtained using the SWIDAC code in other applications, it gave results within 1% of those obtained using the contour shown in Figure 12.

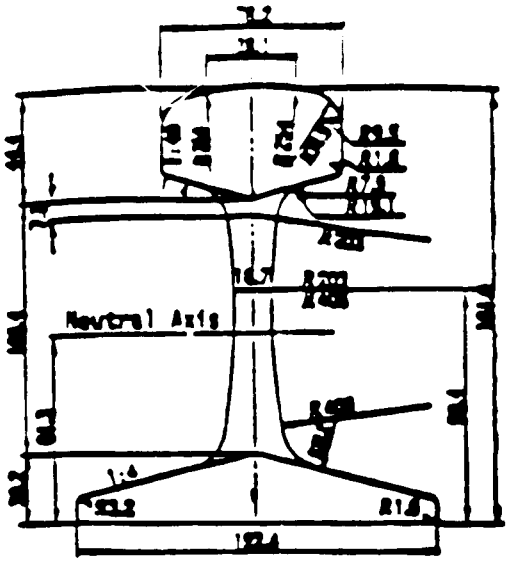

(a) Dimensions of NKKK Rail Cross-Section

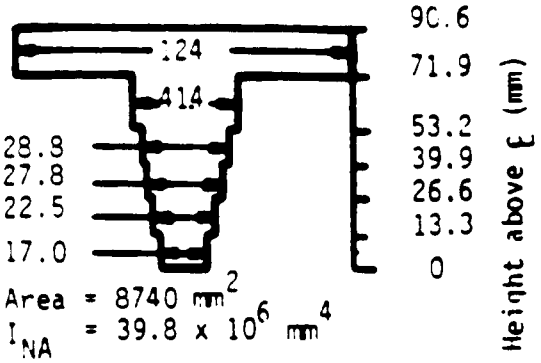

(b) Dimensions of "Equivalent" Symmetric Cross-Section

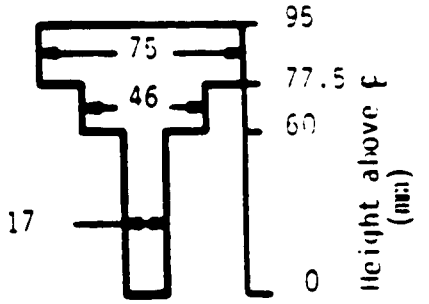

(c) Dimensions of Cross-Section Used in Preliminary Analyses

Figure 11. Comparison of Rail Cross-Sections Used in the Finite Element Analyses of the NKKK Full-Section Impact Tests

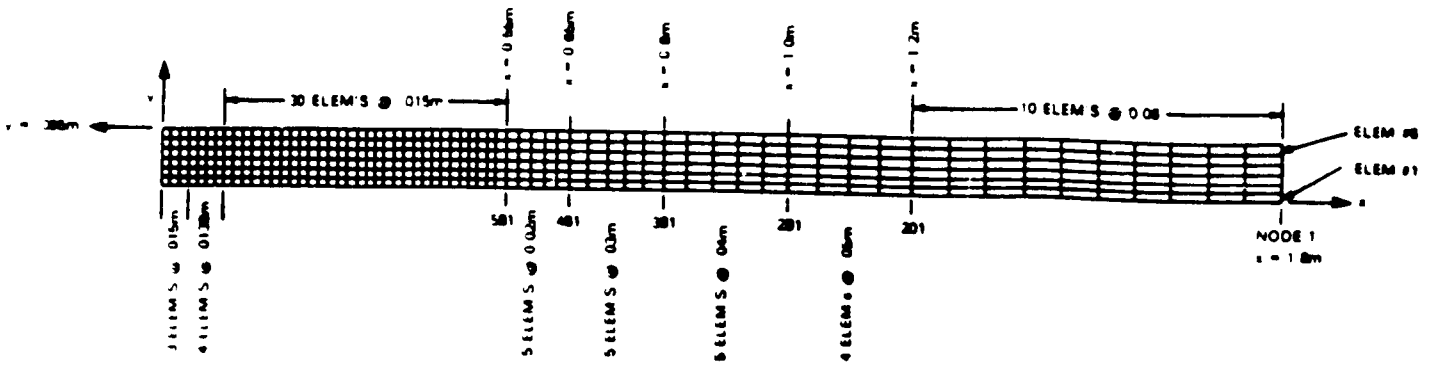

(a) Complete Finite Element Model

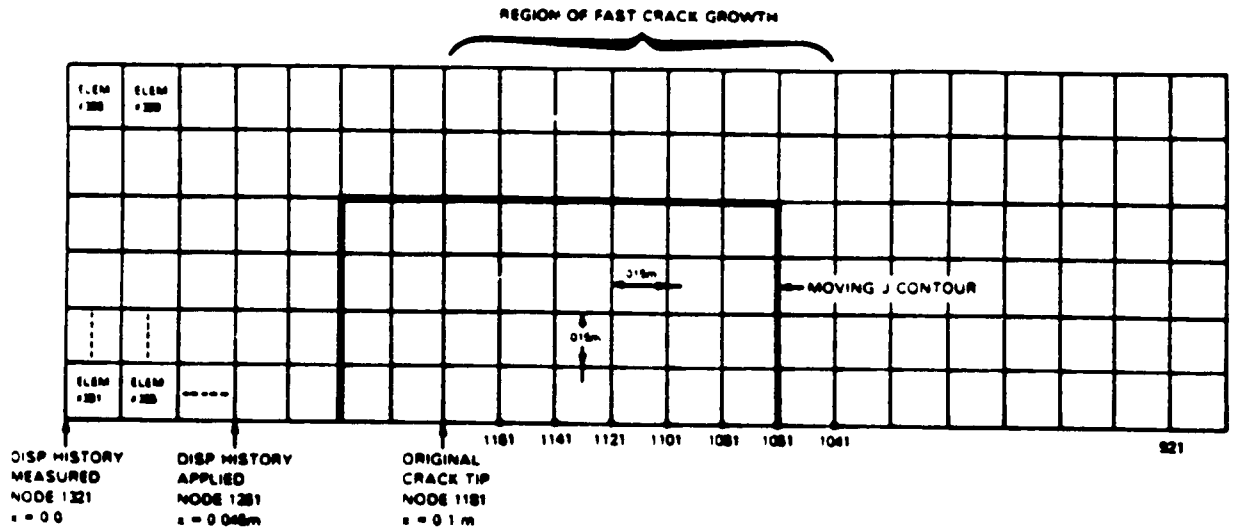

(b) Enlargement of Left Hand End of Model

Figure 12. Mesh for Finite Element Analysis of NKKK Full-Section Impact Test

3.2 Generation-Phase Analysis Results

A generation-phase analysis was performed using one of the NKKK experimental crack length and load-line displacement histories for STDC steel as input to the elastodynamic model of the test specimen. The particular case that was selected is that of the STDC steel experiment shown in Figure 6(b); see also Table 3. Note that while the crack length history is available only for 200 mm of crack extension, the arrested crack length recorded in this experiment was actually 518 mm. Thus, it was not possible to perform the generation phase analysis for the entire event.

The experimental crack opening displacement record obtained from NKKK from their test on the STDC steel at 10°C with an 1800 mm drop height and a 25 Kg drop weight was shown in Figure 8(a). In interpreting this record, it was necessary to extrapolate the record back to a point of zero displacement at the instant of impact; i.e., this point was not shown in the NKKK record. The estimate obtained in this way suggests that the instant of impact occurred 585 μsec prior to the trigger time. The crack length-time data were adjusted to this new time origin accordingly. Specifically, the inputs to the finite element model were actually 585 μs greater than each time given in Table 3.

The crack velocities as a function of crack extension that were obtained from the data supplied by NKKK are shown in Figure 13. Note that the crack extends through the first 15 mm at a very slow (near zero) velocity. This is done because the code requires some crack extension at all times. Consequently, the first element is released slowly to simulate the initial 950 μs period where no crack extension actually occurred. However, beyond 15 mm, the crack velocity used corresponds closely with the NKKK experimental measurements; e.g., an average velocity of about 500 m/s in the interval from 20 to 50 mm of crack extension. It should be noted that the trigger time was only estimated by NKKK. So, the velocity between the trigger and first gage is also just an estimate. However, based on experience with similar experiments, the velocity was probably at least 500 m/s in this interval.

The inferred K_{ID} values as a function of crack extension and of time, respectively, are shown in either Figure 14 and 15. It can be seen that, as the displacement increased prior to rapid crack extension, the driving force increased to about 120 $MPam^{\frac{1}{2}}$. While this is well above the K_{Id} (dynamic initiation toughness) values for rail steel, it is consistent with initiation values for a blunt initial crack as used in the NKKK work. Note that, for convenience in understanding these results, the points A and B denote the same conditions in Figure 14 as in Figure 15.

Figures 14 and 15 also show that the driving force oscillates somewhat under a low value of 20 $MPam^{\frac{1}{2}}$ towards the end of the event. Beyond this point crack growth is probably a series of short crack jumps and/or slow tearing events that may be heavily influenced by residual stresses. In any event, the elastodynamic analysis cannot realistically be applied in this regime. Therefore, the analysis was stopped at this point and only the data from the rapid propagation phase were examined. The resulting K_{ID} vs. velocity data are given in Figure 16.

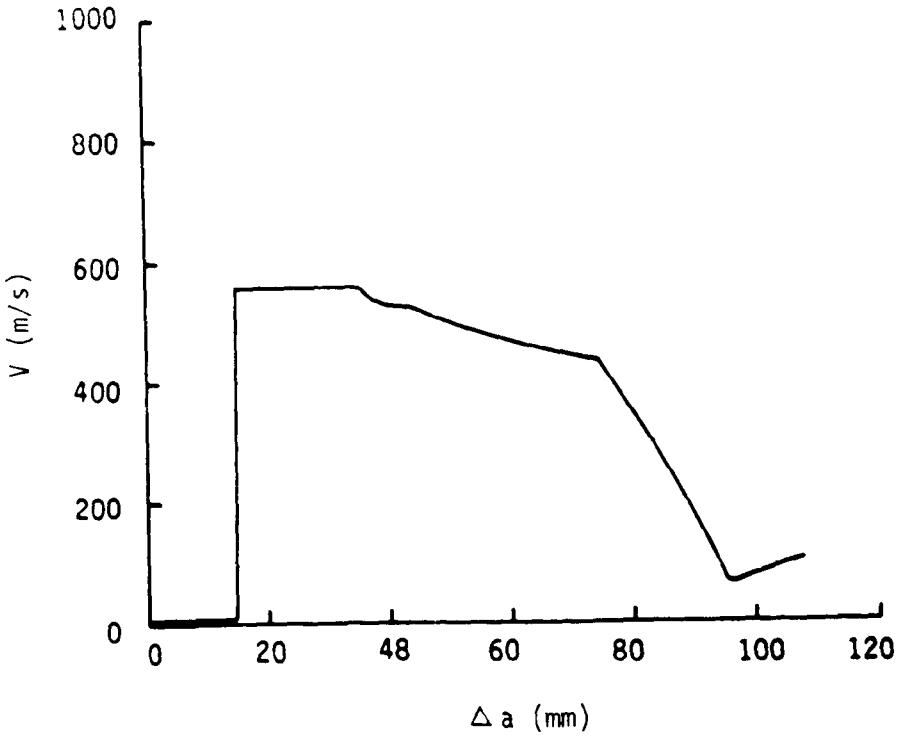

Figure 13. Crack Velocity Versus Crack Extension Deduced for NKKK Test on STDC Steel (10°C) for 25 Kg Dropped from 1800mm.

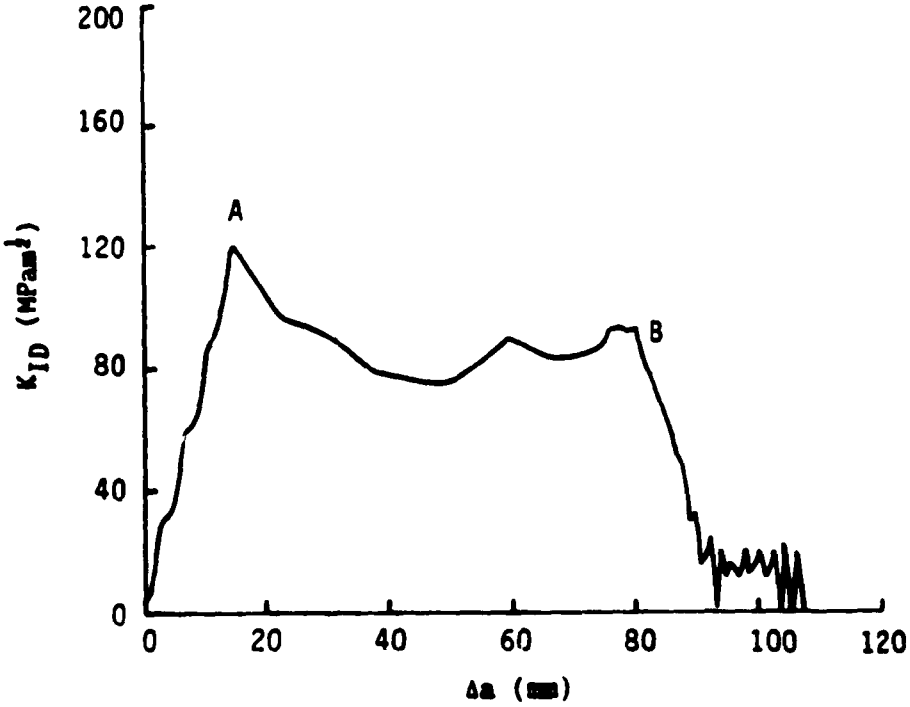

Figure 14. Computed K_{ID} Versus Crack Extension for NKKK Test on STDC Steel (10°C) With 25 Kg Dropped From 1800mm.

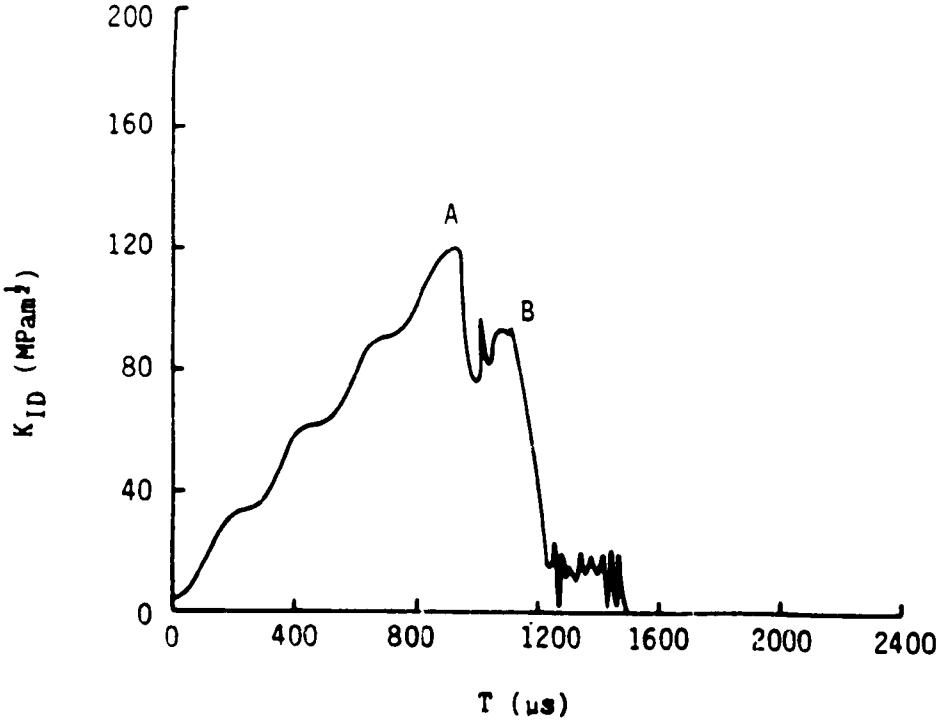

Figure 15. Computed K_{ID} Versus Time for NKKK Test on STDC Steel (10°C) With 25 Kg Dropped From 1800mm.

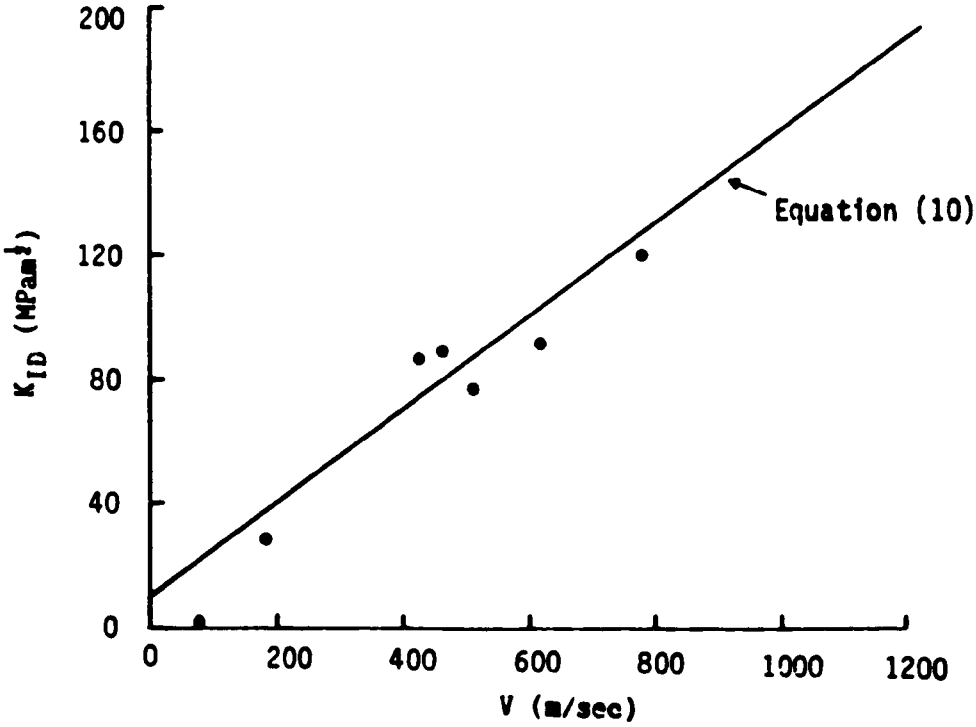

Figure 16. K_{ID} Versus Crack Velocity for STDC Steel at 10°C; Residual Stresses Ignored.

Shown in Figure 16 is a reasonable approximate fit to these data obtained by taking m = 1; cf, Equation (5). This empirical equation is given as:

$$K_{ID} = 10 + 0.150V \qquad (10)$$

where K_{ID} is the propagating fracture toughness in $MPam^{1/2}$ and V is the instantaneous crack speed in m/s. It is important to recognize that, to this point in the work, residual stresses have been ignored. Accordingly, assuming that residual stresses would be tensile in the direction normal to the crack, Equation (10) is an underestimate of the actual dynamic fracture toughnesses. It is for this reason that the constant in Equation (10) differs so significantly from the K_{Ia} value of 29 $MPam^{\frac{1}{2}}$ deduced in Section 2.5.

3.3 Application-Phase Consistency Analysis

As described in Section 2.2, a K_{ID} relation that is inferred from a generation-phase analysis can be taken as a material property in an application-phase analysis wherein the crack-length is calculated as a function of time. These results can then be compared to the experimental measurements to assess the veracity of the approach. Hence, as a consistency check, the first application phase analysis attempted to reproduce the experiment used in the generation-phase analysis described in Section 3.2.

To perform this analysis, the finite element model was loaded with the measured NKKK displacement history; see Figure 8(a). The predicted crack length versus time so obtained is shown in Figure 17. Along with the measured crack length versus time. It can be seen that the rapid crack extension prior to 140 mm is predicted reasonably well. This indicates that the finite element model is correct and, more importantly, that Equation (10) is acceptable. However, the final crack length in the experiment was reported by NKKK to be 518 mm, while the analysis predicts crack arrest at 140 mm.

Several rationalizations for the discrepancy at arrest are conceivable. The most likely is that the crack did indeed arrest at about 140 mm, but then reinitiated and propagated in a quasi-static manner under the combined influence of continued load point displacement increases and residual stresses. Obviously, such a process would only be possible if residual stresses are present and act such as to produce a significant increase in the stress intensity factor. This is believed to be the case on the basis of the work described in Section 4 and the following argument.

In the experiment of Figure 17, the striker was dropped from 1800 mm. It therefore was traveling at about 5.9 m/s as it struck the wedge. The wedge is tapered at 5°, so that, if it were free-falling, the relative separation of the two halves of the specimen would be 1.04 m/s. The rate of change of displacement in Figure 8(a) is 1.03 m/s, suggesting that the wedge was relatively unimpeded. While this would be possible with an extremely well-lubricated wedge and a very compliant material, as discussed in the subsequent section, it is more likely that longitudinal web residual stresses cause the rapid opening of the crack and lead to an apparent free-fall of the wedge. This is consistent with the suggestion that the primary driving force in the latter portion of the experiment arises from residual stresses.

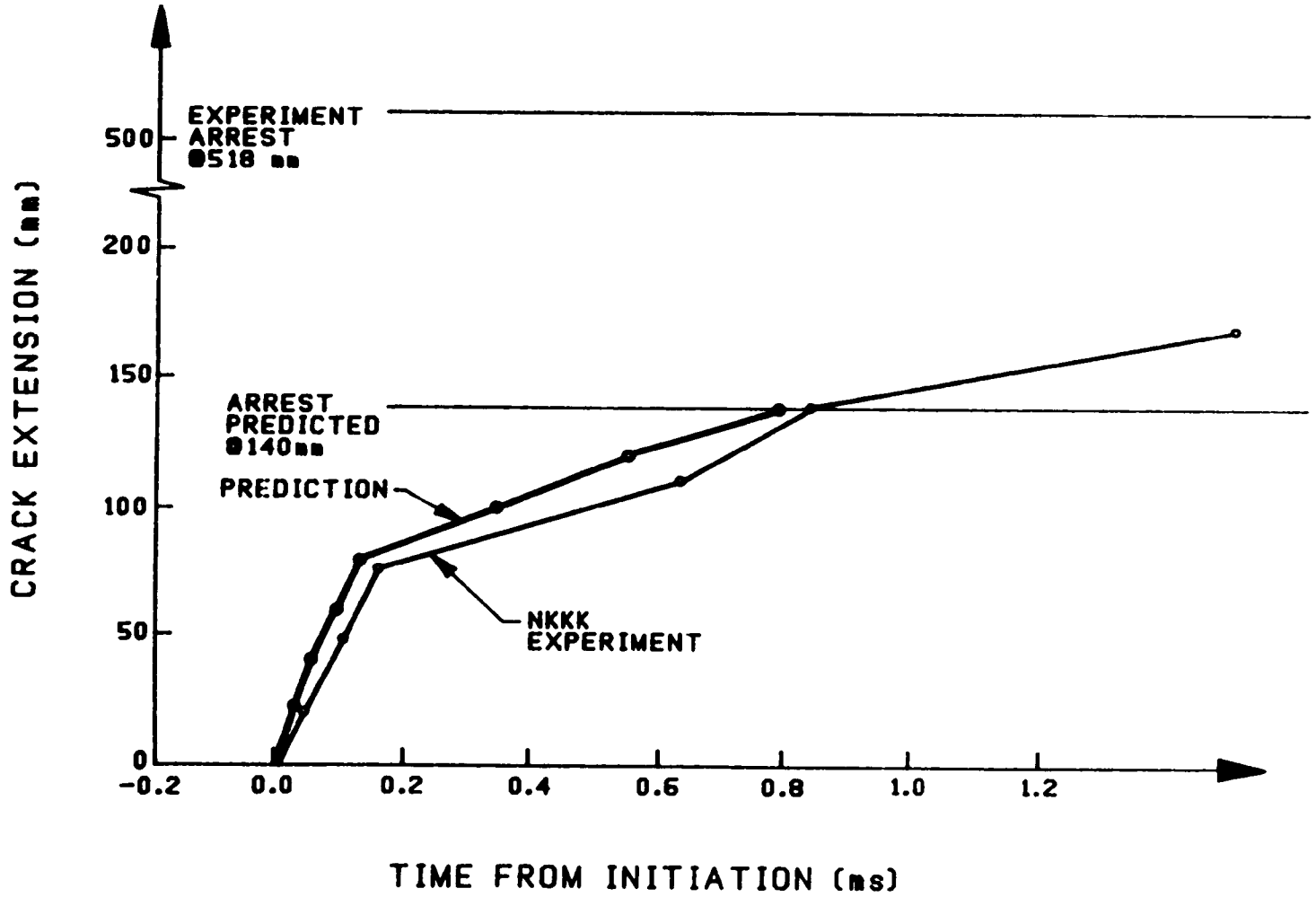

Figure 17. Comparison of Predicted and Observed Crack Propagation on NKKK STDC Steel Full-Section Impact Test at 10°C (25 Kg Drop Weight, 1800 mm Drop Height).

As explained more fully in Section 4, the likely scenario that emerges from this reasoning is that the NKKK full section impact test arrest considered in this section was achieved in two distinct phases. First, rapid crack propagation occurred from the blunted initial crack to 140 mm. Then, a quasi-static (but still rapid) sequence of run arrest events dominated by residual stresses ensued to push the crack to 518 mm in length.

3.4 Application-Phase Analysis Prediction

A second application-phase analysis was performed for an experiment on the same rail steel at the same temperature (i.e., NKKK Rail STDC at 10°C), but for one in which the wedge was dropped from a height of 900 mm as opposed to 1800 mm as in the previously described experiment. This experiment is shown in Figure 6(a). Unfortunately, no record of the displacement for this experiment was available for this analysis. As an expedient, it was assumed that, since the wedge was dropped from half the height, the slope of the displacement versus time should be proportional to that in the previously described experiment by $\sqrt{0.5}$. Using Equation (10) as input, the computed crack length versus time using this assumption is shown in Figure 18.

The result shown in Figure 18 is similar to that shown in Figure 17 except that the predicted final crack length is 130 mm. Perhaps fortuitously, the agreement is better with the experimentally measured final crack length which was 202 mm. It is possible that the residual stresses in this rail were significantly lower than in the companion experiment. However, the more plausible explanation is that the residual stresses were more or less the same in the two rails, but that the interplay between the lower load produced by a smaller drop height and the residual stresses produces a considerably smaller quasi-static crack growth segment.

Refinements in the analysis would surely provide results that agree closer with the crack velocities observed experimentally. For this purpose, more detailed information concerning the timing of the measurements, the residual stresses, the penetration of the split pin, and the crack opening measurement location would be helpful and will be sought. However, of most importance is the effect of the residual stresses. While these could be taken into account, unfortunately, accurate data do not exist whereby unequivocal estimates of these stresses can be made. However, because of the clear importance of residual stresses, the following sections will describe some estimates and their consequences to enable qualitative comparisons with rail fracture experimental results.

3.5 Residual Stress States in Rails

To obtain a preliminary assessment of the importance of residual stresses in a rail web, a static analysis was performed of an initially stress-free split rail that was wedged open. The results are shown as load case 1 in Table 5. The principal stress is normal to the crack line, as expected, with the principal stresses in the upper half of the rail normal to a plane that is rotated slightly clockwise from the crack plane. Therefore, a crack that curved upwards by some local perturbation would be redirected downwards, while a crack that deviated downwards would be redirected upward. It follows that, in the absence of residual stresses, the crack should always propagate in a plane parallel to the head and base of the rail.

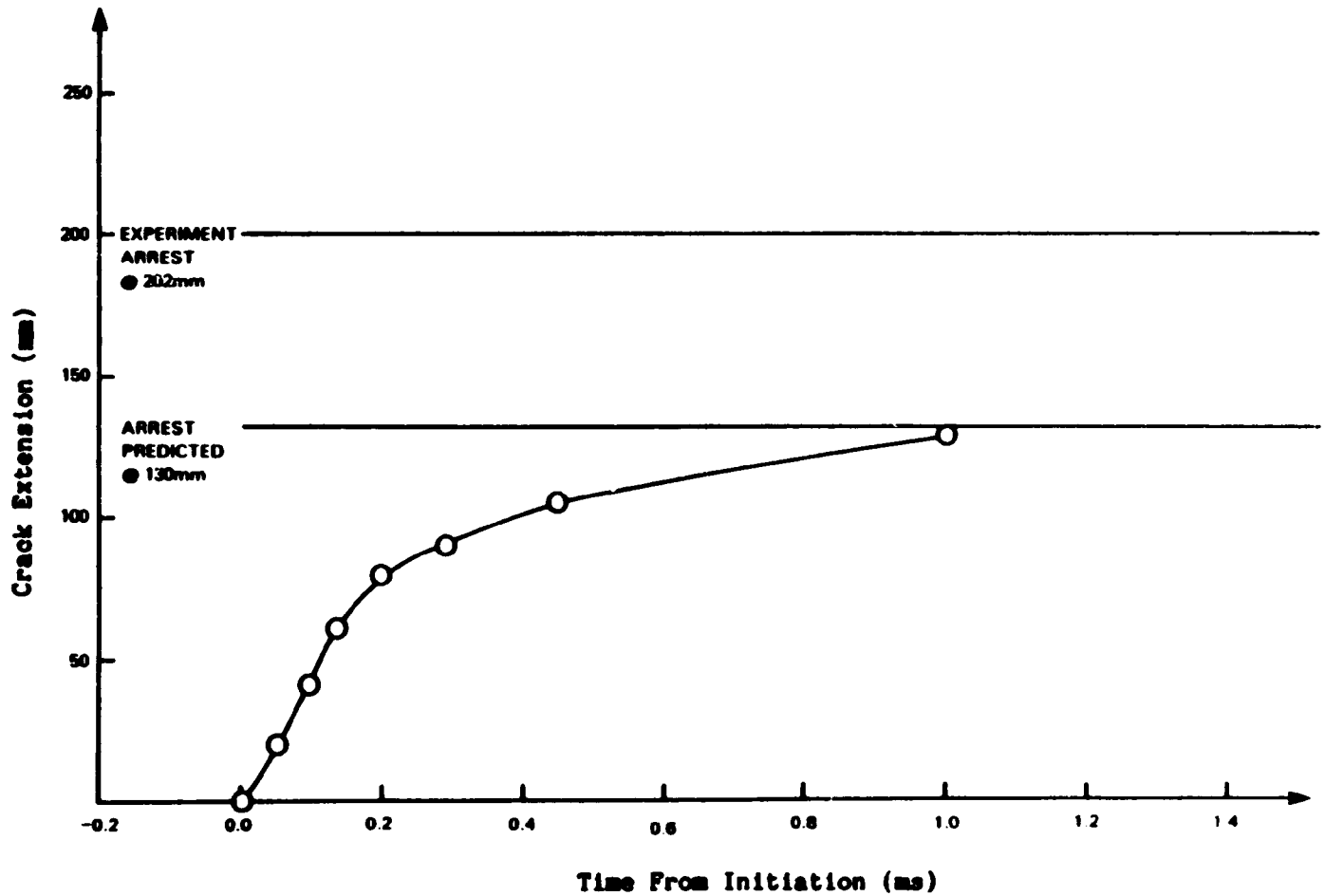

Figure 18. Comparison of Predicted and Observed Crack Lengths in NKKK STDC Steel Full-Section Impact Test at 10°C (25 Kg Drop Weight, 900 mm Drop Height).

Next, longitudinal residual stresses were included in the finite element analysis by applying a temperature gradient from rail head to mid-height. Figure 9 suggests the approximation that longitudinal residual stresses be compressive in the rail head and base, and tensile in the web. Residual stresses of this type would create negligible transverse stresses and therefore add little to the calculated stress intensities. This type of stress distribution differs from the findings of others; NB, see Figure 10. However, accepting it for the moment, a possible explanation of crack curving in some NKKK tests emerges.

Load cases 2 and 3 in Table 5 show the stresses near the crack tip from static finite element analysis with (1) tensile web longitudinal stress and (2) either a small or a large static load applied at the wedge. It can be seen that the direction of the primary stress and the divergence of the crack out of plane depends on the sign of the shear stress. This depends on the external load. Nevertheless, this simple analysis demonstrates that it is likely that the crack will curve when the residual stress state corresponds to that shown in Figure 9. And, as Figure 6(c) shows, this actually occurs.

The results shown in Figure 10, supported by the data of Reference [21], indicate that for standard rail steel the residual stresses are generally compressive in the web and tensile in the head and base. When these rails are saw cut, they open as the web compression relaxes. An uncut rail has virtually no transverse residual stresses. However, once a cut is introduced, a very large transverse stress arises at the tip of the cut. The half of the rail with compressive web residual stress can be thought of as a cantilever beam with an end moment on an elastic foundation. This phenomenon, which contributes significantly to the stress intensity factor, will not occur when the longitudinal stress is tensile in the web.

Reference [20] reports longitudinal residual stresses that approach 300 MPa. Using this as a possible worst case, the rail specimen was reanalyzed. Load cases 4 and 5 in Table 5 show static results for the stress at a point near the crack tip, with and without a load applied at the wedge. It is seen that for both cases a crack would have to remain in plane. Therefore, while compressive web residual stresses contribute strongly to the stress intensity factor, this simple static analysis indicates that it is not possible for the crack to diverge out-of-plane when this condition exists.

3.6 Generation Phase Analyses with Postulated Residual Stresses

Generation phase analyses were first performed with the state of residual stress described by NKKK--see Figure 9. This involves compression in the rail head and tension in the web. However, because tensile longitudinal residual stresses contribute little to the crack driving force, there was essentially no difference between these results and the results described in Section 3.2. However, if the analysis is performed with compressive web longitudinal stresses--i.e., as described in Reference [20]--the K_{IO} results are significantly different. The computed K_{IO} versus crack velocity is shown in Figure 19. For comparison with the results obtained by ignoring residual stresses, the linear relation developed in that analysis, Equation (10), is also shown in Figure 19.

Table 5. Results of Static Analyses Showing Conditions Necessary for Crack Curving

Load Case	Stress at a Point Just Above and in Front of Crack Tip				
	σ_y	σ_x	τ_{xy}	θ_p	Result
1	37	27	10	32°	Remained in plane
2	20	68	-45	-68°	Curved out of plane
3	1210	957	329	35°	Remained in plane
4	690	467	220	32°	Remained in plane
5	1261	894	385	32°	Remained in plane

Load Cases

1. No residual stress, small load applied at wedge.
2. Tensile web residual stress, small load applied at wedge.
3. Tensile web residual stress, large load applied at wedge.
4. Compressive web residual stress, small load applied at wedge.
5. Compressive web residual stress, large load applied at wedge.

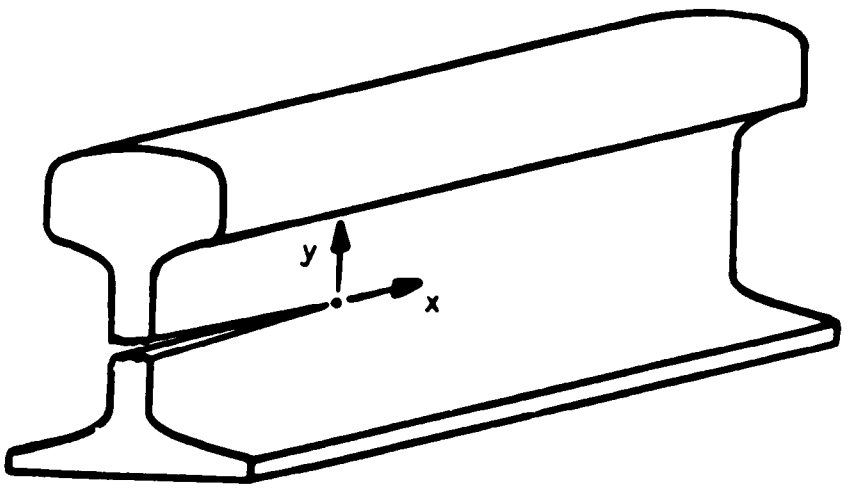

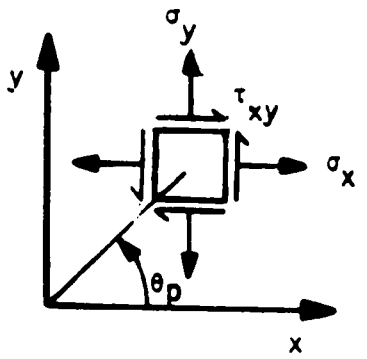

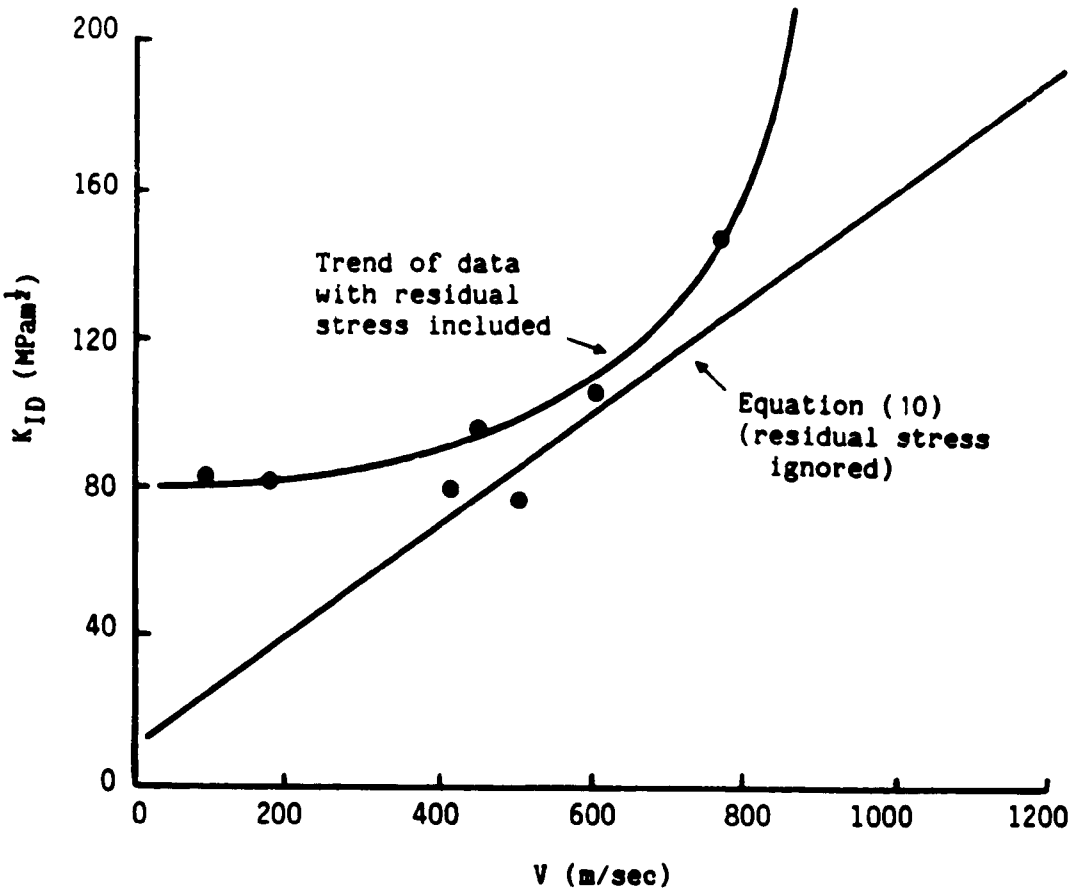

Figure 19. K_{ID} Versus Crack Velocity From a Generation-Phase Analysis of STDC Steel (25 Kg, 1.8 m) at 10°C, with Residual Stress as estimated from Reference [20]. Equation (10), developed without consideration of residual stresses, is shown for comparison.

The data shown in Figure 19 were derived by considering only the first 100 mm of rapid crack growth for the NKKK Test shown in Figure 6(b) and by assuming the residual stresses were as high as 300 MPa. It can be seen that, at lower velocities the computed K_{ID} values are considerably higher than those previously computed without residual stress. Specifically, this analysis indicates that K_{Ia} would be 80 MPam$^{\frac{1}{2}}$. While this is considerably above the values that would be expected (see Section 2.5), there are reasons why this result should not be taken too seriously.

In particular, in this analysis, the wedge lost contact with the rail shortly after crack initiation whereupon, acted upon by the relaxing residual stresses, the specimen opened up with no applied load. Of more importance, the residual stresses for the NKKK experiments may be very different than has been assumed here; i.e., a worst case residual stress was assumed which is likely much different than that in the NKKK experiments.

3.7 Comments on the Finite Element Computations

Because of the geometric complexity of a rail web fracture, as an expedient, the rail was taken to be symmetric. While clearly not physically correct, such an approximation is not felt to be inappropriate at this preliminary stage of the work. More important by far is the current inability to accurately model the state of residual stresses that have been induced in the rail by straightening operations. However, despite these shortcomings, some important findings have emerged from the finite element analyses described in this section.

It was found through the combination of generation-phase and application-phase analyses of the NKKK full-section impact tests that elastodynamic fracture mechanics is appropriate provided (1) a residual stress-dependent dynamic fracture toughness property is used, and (2) the analysis is confined to the initial portion of the total run/arrest event. These findings lead to the obvious conclusion that the residual stresses are of great importance in dictating whether or not a long-running web fracture can occur. Refining this conclusion, static finite element analyses were performed that suggest that tensile longitudinal web residual stresses will give rise to crack curving and abrupt arrest, thereby precluding a long-running fracture. In contrast, compressive longitudinal web residual stresses promote a long-running fracture.

Of perhaps most significance, the elastodynamic finite element computations indicate that the nature of the run/arrest event in a full-section impact test is considerably more complex than expected. That is, the initial dynamic crack propagation appears to be followed by sequential quasi-static run/pause events. While both regimes are highly influenced by the residual stresses, the effect is likely to be different in one regime than in the other. It must be concluded that the raw sum of the crack advance observed in the two regimes - taken in isolation - may not be an appropriate indicator of the potential of a given rail to resist a long-running fracture. The use of a full-section impact test for other than simple screening of rails therefore requires more precise instrumentation and fracture mechanics interpretation.

4. A FRACTURE MECHANICS ANALYSIS FOR RAILS WITH RESIDUAL STRESSES

In the work described in the preceding section, it was not possible to clearly delineate the effects of the toughness properties of the material from the residual stresses. Some simple analyses can be performed for further insight by developing expressions for the stress intensity factor for a crack that has propagated longitudinally along the web of a rail due to residual stresses. As shown in this section, this relation can be obtained through the use of the beam-on-elastic foundation (BOEF) model.

4.1 Quasi-Static Analysis of the Full-Section Rail Impact Test

To obtain a suitable stress intensity factor expression for quasi-static crack growth in a full-section impact test, two modifications were introduced into the BOEF model originated by Kanninen [23]. First, the restriction to a rectangular cross section was removed; second, the effect of web longitudinal residual stresses was incorporated. In so doing, for convenience here, the more general geometric treatment of Reference [23] was specialized to that for a crack that is very long compared to the height of the rail. The derivation is provided in the Appendix to this report.

The key result obtained from the work outlined in the Appendix is that for the stress intensity factor for a crack of length a acted upon by a load point displacement δ and a residual moment M_R. Further invoking a simple assumption to relate M_R to σ_R, the maximum longitudinal (compressive!) residual stress, K for the full-section impact test is

$$K = \left(\frac{I}{b}\right)^{\frac{1}{2}} \frac{\sigma_R}{c} + 3\left(\frac{I}{b}\right)^{\frac{1}{2}} \frac{E\delta}{a^2} \qquad (11)$$

where b is the thickness of the rail web, I is the moment of inertia of the upper portion of a longitudinally split rail, and c is the distance from the crack plane to the centroid of the upper half-rail. Note that, because the vertical constraint that exists in track is absent in a full-section impact test, this result differs from that appropriate for track; see Section 4.4.

Orringer and Tong [1], arguing from a stability standpoint, have also deduced that the residual stress intensity factor must be crack-length independent. However, they did not quantify their conclusion for a split rail geometry. Equation (11) thus uniquely provides a quantitative result for a rail web crack with residual stresses.

The second term on the right hand side of Equation (11) is readily recognizable as a generalization of the usual static stress intensity factor for beam-like geometries in displacement control [23]. Under a fixed or slowly varying displacement, this contribution will vanish for very long crack lengths. In contrast, the first term of Equation (11), which arises from the presence of transverse compressive residual stresses in the web, can be seen to be independent of the crack length. It follows that, for a very long crack, the K value given by the residual stress will become dominant. Hence, as the residual stresses are apparently constant along the rail except near the ends [1], cracks can be driven to virtually complete fracture without any external loading, beyond that needed to initiate unstable crack propagation.

4.2 Elucidation of Run/Pause Sequences in Full-Section Impact Tests

One essential difference between a full-section impact test and actual track service is that, while the load point displacement in the former monotonically increases during much of the crack propagation event, such large increases cannot be expected in track. Recognizing this, equation (11) can be used to support the understanding of the nature of the fracture event in a full-section impact test that was deduced from the finite element results obtained in Section 3 of this report. The initial rapid propagation portion of the event is unquestionably dynamic. However, as it is likely that the latter portion is quasi-static, then, just as appears to be reflected in the NKKK experimental results--see Figure 17--the application of Equation (11) would definitely give rise to a regime of relatively slow crack growth. Figure 20 provides a schematic illustration of how crack growth of this kind would occur through a sequence of run/pause events, as follows.

Let Point A_1 in Figure 20 denote the point of arrest determined by setting $K(a_1, \delta_1) = K_{Ia}$, where the left hand side denotes the stress intensity factor calculated for a crack length a_1 and a load point displacement δ_1. The crack tip will be stationary following this arrest even though the load point displacement may be increasing. However, when the point I_2 in Figure 20 is reached, $K(a_1, \delta_2) = K_{Ic}$, whereupon rapid propagation is re-initiated. The subsequent run event is then arrested at A_2 where $K(a_2, \delta_2) = K_{Ia}$. This completes one run/arrest cycle. Depending upon the relative values of K_{Ic}, K_{Ia} and K_R (the contribution of the residual stresses) and the maximum δ value that is achieved in a full section impact test, the run/arrest sequence could continue until either complete fracture occurs or a stable arrest is attained.

Note that this scenario is predicated on the assumption that $K_{Ia} > K_R$. If instead $K_{Ia} < K_R$, unstable fracture will occur. In the former instance, it is clear that, when the residual stresses provide a significant contribution to the crack driving force in a full-section impact test, a crack that is initiated at a blunt crack undergoes two distinct phases: rapid propagation to a temporary arrest followed by a period of sequential short run/pause events. It follows that the total crack propagation distance observed in a full-section impact test does not provide a clear cut indication of the inherent fracture toughness, the residual stresses, or of their combination.

4.3 Suggested Basis for Rail Integrity Assessments

The crack length-independent term in Equation (11) helps to explain both the derailment accident resulting from the catastrophic fracture shown in Figure 1, and an unrelated fracture incident on the same steel described in Reference [1]. In the latter, a premium alloy rail experienced rapid web fracture from having been accidentally dropped prior to track service. In the absence of residual stresses, the initial impact would be utterly inadequate to propagate the crack more than a very short distance, much less through the entire length of the rail. However, as Equation (11) reveals, once initiated, a long-running fracture is clearly possible.

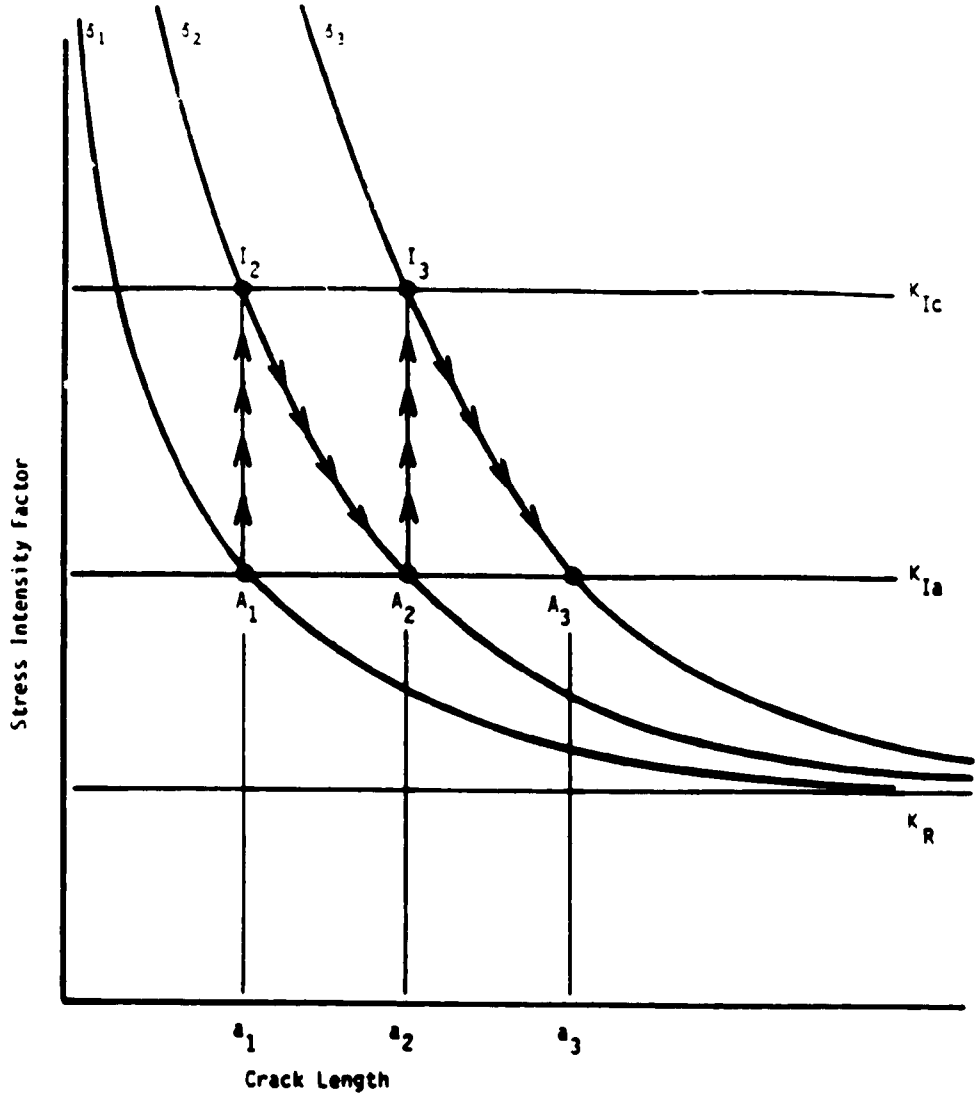

Figure 20. Conceptual Illustration of Sequential Quasi-Static Run/Pause Segments in the Terminal Phase of a Full-Section Impact Test.

The analysis techniques employed in this work are capable of delineating the interaction that would allow the full-section impact test to be used as an indicator of rail fracture propensity, albeit in a more meaningful (and complicated) manner than at present. An appropriate basis for a quantitative understanding of rail integrity via crack arrest is provided by a generalization of Equation (2). More specifically, for cracks that propagate in a straight line, the work reported herein has made clear that three distinct contributions to a long-running web crack exist and can be quantified. As suggested by Equation (11), the kinetic relation for fast crack propagation in a rail can be expressed as

$$K(a,t) = K_{ID}(V,T) - K_R \tag{12}$$

where K denotes the dynamically computed crack driving force for the load and crack length of interest, while the right hand side denotes a pseudo-toughness; i.e., the combined effect of the inherent fracture toughness of the rail steel and the residual stress contribution, K_R; NB, this approach was tacitly adopted in the computations that led to Equation (10).

Alternatively, in terms of Equation (12), the arrest condition given by Inequality (3) can be extended to

$$K_{max} + K_R < K_{Ia} \tag{13}$$

where K_{max} denotes the maximum externally-imposed crack driving force; e.g., from wheel loads. Thus, provided K_R and K_{Ia} can each be evaluated for the rail of interest, Inequality (13) provides a practical basis for evaluating the arrestability of that rail for service conditions; i.e., through K_{max} values analogous to those developed for gas transmission pipelines (see Section 2.4).

For present purposes it will be assumed that the residual stresses provide the only contribution to driving a long-running web crack. It is then only necessary to employ an expression for the dynamic stress intensity factor for steady-state dynamic crack propagation under a constant residual moment. As shown in the Appendix, if no external forces are acting on the cracked rail, this expression can also be obtained from the beam-on-elastic foundation model. The result is

$$K = K_R \left(1 - \frac{V^2}{V_{cr}^2}\right) \tag{14}$$

where V is the crack speed and $V_{cr} = C_o(bI/c)^{\frac{1}{2}}/A$ is a critical crack speed for rail web crack propagation. Here, b, I, and c are as defined in connection with Equation (11) while A is the cross section area of the upper half rail. This result suggests that, in rail, dynamic conditions give rise to lower crack driving forces than occur in static conditions.

4.4 Estimates for Fracture Propagation in Rails

Equation (14) gives the dynamic stress intensity factor for a long-running web crack in track that is driven by residual stresses only. As shown in the appendix, because of the constraint that exists for track, the contribution of the residual stresses differs from that obtained for the full section impact test. The appropriate relation for track is

$$K_R = \frac{\sigma_R}{c}\left(\frac{I}{2b}\right)^{\frac{1}{2}} \tag{15}$$

To assess this relation for rail through the use of actual rail geometry and residual stress data, approximate values were obtained using the rail cross section shown in Figure 11. Note that, consistent with the split rail analysis using the beam-on-elastic-foundation model, the following values are for a half-rail.

$$b = 17 \text{ mm}$$
$$c = 59 \text{ mm}$$
$$h = 85 \text{ mm}$$
$$A = 4370 \text{ mm}^2$$
$$I = 3\times10^6 \text{ mm}^4$$

Use of these values leads to V_{cr} = 1100 m/sec (see Equation 14) in which the value C_o = 5190 m/sec for steel was used [5]. Next, for convenience, Equation (15) can be written as

$$K_R = 0.159\sigma_R \tag{16}$$

Note that σ_R must be in MPa to give K_R in $MPam^{\frac{1}{2}}$.

From Figure 10, it can be seen that σ_R values range from 50 to 200 MPa. For σ_R=150 Mpa, which represents a typical value, K_R = 24 $MPam^{\frac{1}{2}}$. This value can be compared with the K_{Ia} values for rail estimated in Section 2.5. Of particular interest are the values of 29 $MPam^{\frac{1}{2}}$ for standard rail and 17 $MPam^{\frac{1}{2}}$ for the failed rail. It should of course be recognized that these are <u>average</u> values. It is nonetheless of interest to compare them with the crack driving forces that have been deduced.

Because a long-running crack is not likely to be possible if $K_{Ia} > K_R$, these values indicate that a long-running crack driven by residual stresses alone would not likely occur for standard rail. In contrast, as a long-running crack could occur if $K_{Ia} < K_R$, these values indicate that such an event could indeed occur for the failed rail.

Alternatively, for a given rail steel, one might want to estimate the maximum permissible rail web compressive residual stress that could exist without the danger of a long-running fracture. In so doing, the wide range of crack arrest toughness values that could exist should be considered. This is illustrated in Figure 21 which shows K_R as a function of σ_R obtained from Equation (16) together with the K_{Ia} values estimated in Section 2.5. It can be seen that the K_{Ia} values for standard rail steel range from 20 to 34 MPam$^{\frac{1}{2}}$. Using the lower level of these data, the maximum permissible value of σ_R would be 126 MPa. Also, for the failed rail, σ_R should have been less than 107 MPa.

Using Equation (14), it is further possible to obtain an estimate for the crack propagation speed in a rail having a speed-independent dynamic fracture toughness value equal to its K_{Ia} value; i.e., if the speed-dependent portion of Equation (5) is neglected then $K_{ID} = K_{Ia}$. The result is

$$V = V_{cr}\left[1 - \frac{K_{Ia}}{K_R}\right]^{\frac{1}{2}} \tag{17}$$

For the failed rail, assuming K_{Ia} = 17 MPam$^{\frac{1}{2}}$ and σ_R=150 MPa, Equation (17) gives V=600 m/sec. Alternatively, using K_{Ia} = 20 MPam$^{\frac{1}{2}}$ (see Table 4), V would be 440 m/sec. This implies that the 10 meter length of rail was fractured in about 20 ms.

These calculated crack speeds can be compared with the speed of the train that initiated the accident [1]. This was was 32 m/sec (72 mph). That the crack speed is significantly greater than the train speed is consistent with the basic assumption that, while mechanical stresses likely served to initiate crack propagation, the long-running crack was essentially driven by residual stresses only.

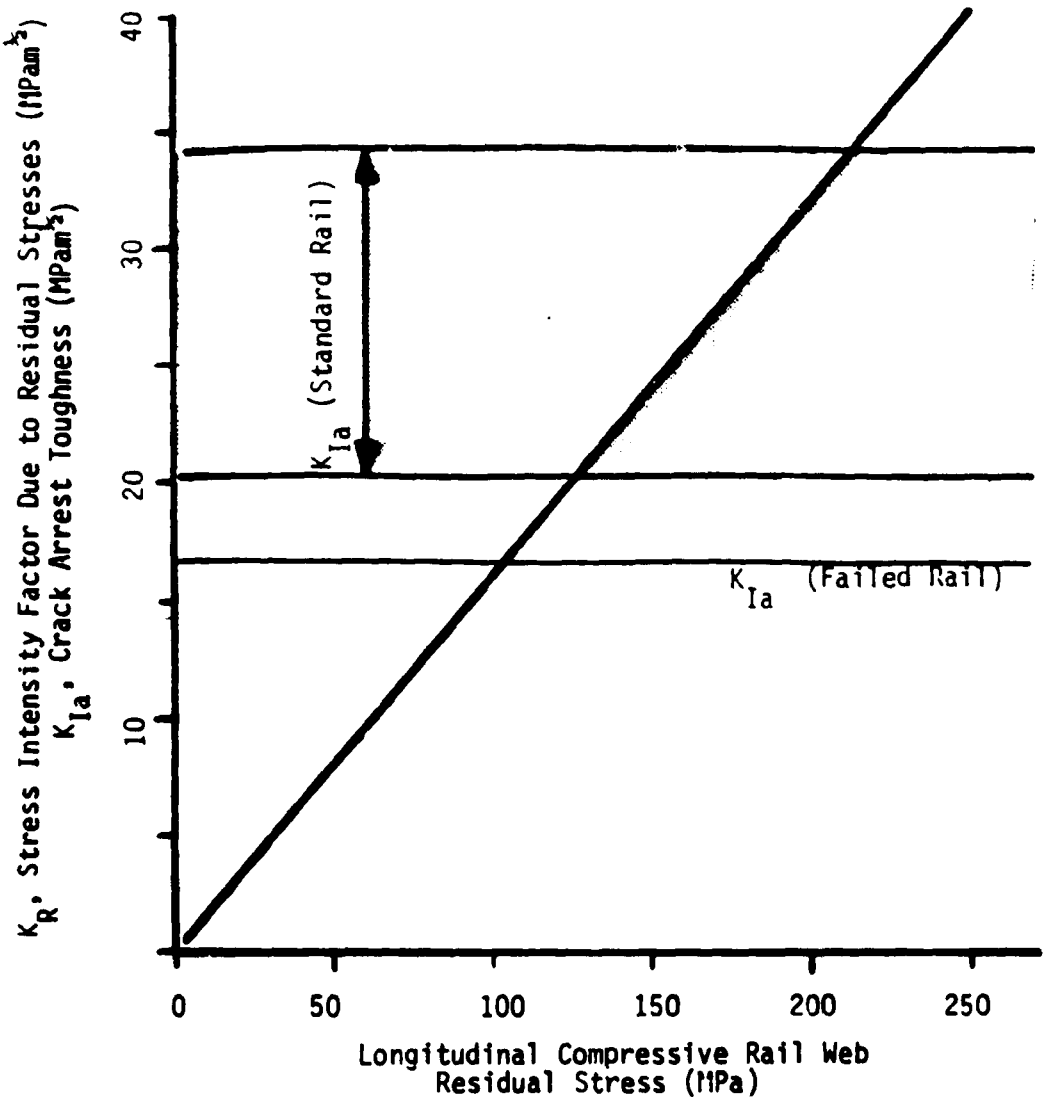

Figure 21. Tentative Basis for the Assessment of the Potential for a Long-Running Fracture in Rails with Compressive Longitudinal Web Residual Stresses.

5. DISCUSSION AND CONCLUSIONS

The catastrophic rail fracture event in premium-alloy rail that has focused attention on this problem was triggered by a flaw induced by a torch cutting operation [1]. While this was a highly exceptional condition, it is nevertheless prudent to assume that initiation sites always will be present; e.g., from fatigue cracks at bolt holes [24]. Indeed, because of the likelihood that the more wide-spread use of lubricated track will change the governing factor in rail life from wear to fatigue [25], fracture prevention may be even more crucial in the future.

Motivated by these considerations, current dynamic fracture mechanics procedures were employed in this research to obtain a preliminary assessment of the fracture potential of candidate rail steels and the residual stresses arising from straightening operations. Specific attention was placed upon the data from instrumented full-section impact tests on standard rails obtained by NKKK. It was found that the total amount of readily observable crack advance in this type of test may be the sum of two distinctly different events:

(1) rapid crack propagation (e.g., at about 500 m/sec--see Figure 13) dominated by the material dynamic fracture toughness properties, and

(2) sequential run/pause behavior that is heavily influenced by the residual stresses and an increasing load-point displacement.

It follows that both the rail steel dynamic fracture toughness and the residual stresses induced by straightening operations can contribute significantly to driving a long-running crack. However, because the manner in which a full-section impact test is conducted differs significantly from service conditions, the observed total crack advance in a full-section impact test, taken in isolation, is unlikely to be a reliable indicator of service behavior.

It has also been shown here that residual stresses can be of sufficient magnitude to cause a long-running fracture. Accordingly, rail safety assessments need not only rely on precluding the initiation of rapid growth, but should include crack arrest after a short extent of crack propagation (or abrupt crack turning) as second lines of defense against catastrophic fracture.

While the work reported here has served only to initiate the needed research, the ultimate value of the research is clear. First, if instrumented to provide the boundary conditions for fracture mechanics analyses, the full-section impact test can be made to provide the data needed to determine fracture toughness and residual stresses. Second, if estimates of crack driving forces in track are made and combined with these results, effective safety assessments of given rail steels and straightening procedures can be obtained.

6. RECOMMENDATIONS FOR FURTHER RESEARCH

Because the crack driving force arising from typical residual stresses in rail appears to be comparable to the dynamic fracture toughness values of rail steel, the risk of a long-running web fracture is appreciable. It was further concluded from this work that the total crack length experienced in a full-section impact test does not provide a meaningful assessment of this risk. It should nevertheless be recognized that these findings were inferred using fairly simple computational models and less than complete experimental data. Because of the significance of these conclusions to railroad safety, more realistic analyses are therefore needed to affirm them. Accordingly, it is recommended that the research initiated in this report be continued to enable more comprehensive analysis procedures to be developed and applied.

This further research should first seek additional experimental fracture propagation data and residual stress information for various types of rails. Because a complete set of data is unlikely to be already available, instrumented rail fracture experimentation will need to be undertaken. As a key step, it is essential to develop improved finite element analyses of rail to perform more precise computations than have so far been possible. Of most importance, these analyses must incorporate (1) three-dimensional effects, (2) residual stresses, and (3) crack curving. This study would be aimed at obtaining a more decisive assessment of the risk of catastrophic rail web fracture than has so far been possible.

Assuming that the results obtained by the collection of additional data and by analysis approach refinements do not significantly alter the tentative conclusions reached in the present report, a further step would appear to be mandated. That is, because of the delicate balance that appears to exist between the crack driving forces arising from residual stresses induced by straightening operations and the innate fracture toughness values of rail steel, there is a clear need to develop a fracture propagation assessment procedure for rail.

The obvious candidate for the basis of such a procedure is the full-section impact test, instrumented as in the NKKK work. However, while such experimentation could play a key role, it is clear that this procedure would not be acceptable for routine railroad purposes. Accordingly, the ultimate objective of this recommended work would be to develop and validate a simple and reliable "screening" procedure to qualify rail for fracture-safe service; e.g., a compact crack arrest specimen. The analysis techniques that could be developed in the near-term, coupled with judiciously instrumented fracture propagation/arrest experimentation, would make it possible to accomplish this.

7. REFERENCES

[1] Orringer, O. and Tong, P., "Investigation of Catastrophic Failure of a Premium-Alloy Railroad Rail," Fracture Problems in the Transportation Industry, edited by P. Tong and O. Orringer, American Society of Civil Engineers, New York, pp 62-79, 1985.

[2] John, R. R. et al, "Task Force Report on Rail Failure Evaluation," Transportation Systems Center Report to the Federal Railroad Administration, May, 1984.

[3] Anon., "Crack Propagation and Arrest Test on Rail Steels," Nippon Kokan K.K. report, Kawasaki, Japan, March, 1985.

[4] Watanabe, I., and Gino, T., Nippon Kokan K.K., Technical Research Center, Kawasaki, Japan, private communication to M. F. Kanninen, 28 August 1985.

[5] Kanninen, M. F., and Popelar, C. H., Advanced Fracture Mechanics, Chapter 4, Oxford Press, New York, 1985.

[6] Kanninen, M.F., "Applications of Dynamic Fracture Mechanics for the Prediction of Crack Arrest in Engineering Structures," International Journal of Fracture, Vol. 27, pp 299-312, 1985.

[7] Kanninen, M. F., Sampath, S. G., and Popelar, C. H., "Steady-State Crack Propagation in Pressurized Pipelines," Journal of Pressure Vessel Technology Vol. 98, pp. 56-65, 1976.

[8] McGuire, P.A., Sampath, S.G., Popelar, C.H., and Kanninen, M.F., "A Theoretical Model for Crack Arrest in Pressurized Pipelines," Crack Arrest Methodology and Applications, ASTM STP 711, edited by G.T. Hahn and M.F. Kanninen, pp 341-358, 1980.

[9] Kalthoff, J. F., Beinert, J., and Winkler, S., "Measurements of Dynamic Stress Intensity Factors for Fast Running and Arresting Cracks in Double-Cantilever-Beam Specimens," Fast Fracture and Crack Arrest, ASTM STP 627, American Society Testing and Materials, edited by G.T. Hahn and M.F. Kanninen, Philadelphia, pp. 161-176, 1977.

[10] Unpublished results of S.J. Hudak et al, Southwest Research Institute, and A.J. Rosakis et al, California Institute of Technology, June, 1986.

[11] Tetelman, A. S., and Stone, D. H., "An Introduction to the Fracture Mechanics of Rail Material," AAR Report R-157, May, 1974: see Besuner, P.M., "Fracture Mechanics Analysis of Rails with Shell-Initiated Transverse Cracks," ASTM STP 644, edited by D.H. Stone and G.G. Knupp, eds., pp. 303-329, 1978.

[12] Jones, D. J., and Rice, R. C., "Determination of K_{Ic} Fracture Toughness for Alloy Rail Steel," Battelle Columbus Laboratories Report to Transportation Systems Center, Cambridge, MA, 15 November 1985.

[13] Park, Y. J. and Fletcher, F. B., "Fatigue Behavior and Fracture Toughness of Standard Carbon and High Strength Rail Steels," Second International Heavy Haul Railway Conference, Colorado Springs, Colorado, September, 1982.

[14] Kalousek, J., Parsons, D. E. and Ghonem, H., "Effects of 'Streaks' on the Fracture Toughness of Chromium-Molybedenum Rail Steel," Canadian Metallurgical Quarterly, Vol. 21, pp. 25-30, 1982.

[15] Stone, D. H., and Steele, R. K., "The Effect of Mechanical Properties Upon the Performance of Railroad Rails," ASTM STP 644, edited by D. H. Stone and G. G. Knupp, pp. 21-62, 1978.

[16] Marich. S. and Curcio, P., "Development of High-Strength Alloyed Rail Steels Suitable for Heavy Duty Applications," ASTM STP 644, edited by D. H. Stone and G. G. Knupp, pp. 145-166, 1978.

[17] Barsom, J. M., and Imhof, E. J., Jr., "Fatigue and Fracture Behavior of Carbon-Steel Rails," ASTM STP 644, edited by D. H. Stone and G. G. Knupp, pp. 387-413, 1978.

[18] Fowler, G. J., and Tetelman, A. S., "The Effect of Grain Boundary Ferrite on Fatigue Crack Propagation in Pearlitic Rail Steels," ASTM STP 644, D. H. Stone and G. G. Knupp, eds., pp. 363-386, 1978.

[19] McEvily, A.J. and Ochi, Y., University of Connecticut, Storrs, CT., private communication to M.F. Kanninen, 23 June 1986.

[20] Anon, "Factors Influencing the Fracture Resistance of Rails in the Unused Condition," Office for Research and Experiments of the International Union of Railways, Utrecht, Report No. 1, September, 1984.

[21] Rice, R.C., "Determination of Residual Stresses in Alloy Rail Steels," Battelle's Columbus Laboratories letter report to O. Orringer, Transportation Systems Center, Cambridge, MA., 2 July 1985.

[22] Jung, J., Ahmad, J., Kanninen, M. F., Popelar, C.H., "Finite Element Analysis of Dynamic Crack Propagation," Failure Prevention and Reliability, ASME, pp. 7-12, 1981.

[23] Kanninen, M.F., "An Augmented Double Cantilever Beam Model for Studying Crack Propagation and Arrest," International Journal of Fracture, Vol. 9, pp. 83-92, 1973.

[24] Orringer, O., Morris, J.M., and Steele, R.K., "Applied Research on Rail Fatigue and Fracture in the United States," Theoretical and Applied Mechanics, Vol. 1, pp. 23-49, 1984.

[25] Orringer, O. and Steele, R.K., "Structural Integrity of Rail in U.S. Railroad Track," Nineteenth ASTM National Symposium in Fracture Mechanics, San Antonio, Texas, 1 July 1986.

APPENDIX

USE OF A BEAM-ON-ELASTIC FOUNDATION MODEL FOR A RAIL WEB CRACK IN THE PRESENCE OF RESIDUAL STRESSES

A beam-on-elastic foundation (BOEF) model for the double cantilever beam (DCB) test specimen was introduced by Kanninen [23]. Because of the obvious similarities with the rail geometry, this model can also be exploited to develop a relation for the stress intensity factor for a longitudinally split rail in the presence of residual stresses. Outlines of the derivations for quasi-static and dynamic conditions are as follows.

Quasi-static Conditions

For a coordinate system located at the crack tip, the BOEF model at its simplest level requires the development of a solution for $w(x)$, the transverse deflection of the rail as a function of the longitudinal coordinate x. Note that w is associated with the centroid of the half-rail, and that the crack tip is located at the origin. Under these conditions, the governing equation for the BOEF model of a longitudinally split rail is

$$\frac{d^4w}{dx^4} + 4\lambda^4 H(x)\, w = 0 \tag{A.1}$$

in which $H(x)$ is the Heaviside step function and

$$\lambda^4 = \frac{k}{4EI} \tag{A.2}$$

where I is the moment of inertia associated with the upper half of the rail, k is the foundation modulus, and b is the rail web thickness at the crack plane.

As in the DCB specimen, the elastic foundation is here taken to represent the influence of the transverse elasticity of one half of the rail upon the other. It is therefore not an independent parameter but is instead related to the rail dimensions and mechanical properties. For a longitudinally split rail, an approximate relation can be obtained by considering the rail to be symmetric. Specifically, from Hooke's law, $\sigma = kw/b = E\varepsilon = Ew/c$, whereupon it is readily obvious that

$$k = \frac{E\,b}{c} \tag{A.3}$$

where E is elastic modulus of the rail steel, and c is the distance from the crack line to the centroid of the half-rail.*

---

* As the determination of the stress intensity factor is independent of k, the specific assumptions embodied in Equation (A.3) are irrelevant for the purposes of this report. This relation is nevertheless included for clarity and completeness.

The BOEF model has the useful feature that the energy release rate is exactly related to the energy contained in the foundation element at the crack tip; see Advanced Fracture Mechanics, pp 240-246. This can be expressed through the relation

$$G = \frac{p}{2} \frac{k}{b} w_{ct}^2 \tag{A.4}$$

where $w_{ct} = w(o)$ is the transverse displacement at the crack tip and p is a parameter that describes the vertical constraint at the crack tip; i.e., for the unconstrained (symmetric) deformation occuring in a full-section impact test, p = 2, for constrained (nonsymmetric) deformation as in track, p = 1.

Assuming that plane stress conditions describe the overall response of the rail, then $K = (EG)^{\frac{1}{2}}$. Hence, from Equations (A.3) and (A.4)

$$K = \left(\frac{p}{2c}\right)^{\frac{1}{2}} E w_{ct} \tag{A.5}$$

The boundary conditions appropriate for a full-section impact test in a rail with self-equilibrated residual stresses are those arising from a specified load-point displacement δ, and a specified residual moment M_R, both acting at x = -a, where a is the current crack length. The solution of Equation (A.1) that satisfies these boundary conditions and provides quiescent behavior as $x \to \infty$ is readily obtained from that given in reference [23]. Omitting the details, the crack tip deflection can then be found to be

$$w_{ct} = \frac{3}{2} \frac{\delta}{\lambda^2 a^2} + \frac{M_R}{4\lambda^2 EI} \tag{A.6}$$

where, for simplicity, it has been assumed that a>>h, and that p = 2 is appropriate for the full-section impact test.

Substituting Equation (A.6) into Equation (A.5) then gives

$$K = 3E\left(\frac{I}{b}\right)^{\frac{1}{2}} \frac{\delta}{a^2} + \frac{M_R}{(Ib)^{\frac{1}{2}}} \tag{A.7}$$

As a check, consider the special case of a rectangular cross-section. Then, $I = bh^3/12$ whereupon Equation (A.7) reduces to

$$K = \frac{\sqrt{3}\, Eh^{3/2}\delta}{2a^2} + \frac{2\sqrt{3}\, M_R}{bh^{3/2}} \tag{A.8}$$

which agrees with results that are given in Reference [23].

Further progress towards a relation that is useful for practical purposes must admit the longitudinal compressive web residual stress, σ_R. This is readily done if it is assumed that the stress distribution is linear through the rail height. Then

$$M_R = \frac{I\sigma_R}{c} \tag{A.9}$$

Substituting Equation (A.9) into (A.7) then gives

$$K = 3E\left(\frac{I}{b}\right)^{\frac{1}{2}} \frac{\delta}{a^2} + \left(\frac{I}{b}\right)^{\frac{1}{2}} \frac{\sigma_R}{c} \tag{A.10}$$

This is Equation (11) of the main text.

Dynamic Conditions

Equation (A.10) indicates that the effect of a load-point displacement becomes negligible in comparison to the residual stress if the crack becomes very long. If this is so, the crack length disappears from the problem. This suggests that the dynamic crack propagation problem can be addressed through the assumption of steady-state conditions; i.e., through the introduction of the coordinate transformation

$$\xi = x - Vt \tag{A.11}$$

where x denotes the longitudinal position, t is time and V is the steady-state crack speed. Incorporating an inertia term into Equation (A.1) and using (A.11) then leads to the governing equation of motion for steady-state dynamic deflection. This can be written as

$$\frac{d^4w}{d\xi^4} + 4\beta^2 \frac{d^2w}{d\xi^2} + 4\lambda^4 H(\xi)w = 0 \tag{A.12}$$

where

$$\beta^2 = \frac{\rho AV^2}{4EI} \tag{A.13}$$

where ρ is the mass density of the rail steel and A is the cross sectional area of the half-rail. Other symbols are as previously defined.

It will suffice to obtain the solution to Equation (A.12) with boundary conditions representing a constant moment and zero shear stress being imposed at the origin; i.e.,

$$\frac{d^2w}{d\xi^2} = \frac{M_R}{EI} \quad \text{and} \quad \frac{d^3w}{d\xi^3} = 0 \quad \text{at} \quad \xi = 0$$

This solution is given by

$$w(\xi) = \frac{(3m^2-n^2)}{(m^2+n^2)^2} \frac{M_R}{EI} \left[\cos n\xi + \frac{m}{n} \frac{m^2-3n^2}{3m^2-n^2} \sin n\xi \right] e^{-m\xi} \tag{A.14}$$

where

$$m = (\lambda^2-\beta^2)^{\frac{1}{2}}$$
$$n = (\lambda^2+\beta^2)^{\frac{1}{2}} \tag{A.15}$$

It can then be seen that

$$w_{ct} = \frac{\lambda^2-2\beta^2}{2\lambda^4} \frac{M_R}{EI} \tag{A.16}$$

The crack driving force relation given by Equation (A.5) is also appropriate for dynamic conditions. For track, where the opening of the lower half of the rail is constrained, it is appropriate to take p = 1. Then, substitution of Equation (A.16) into (A.5) and the use of (A.2), (A.9) and (A.13) gives a result that can be written as

$$K = \frac{\sigma_R}{c}\left(\frac{I}{2b}\right)^{\frac{1}{2}} \left[1 - \frac{v^2}{v_{cr}^2}\right] \tag{A.17}$$

where V_{cr} is a critical crack speed for rail web crack propagation that is given by

$$V_{cr} = \left(\frac{bI}{c}\right)^{\frac{1}{2}} \frac{C_o}{A} \tag{A.18}$$

where $C_o = \sqrt{E/\rho}$ is the elastic bar wave speed for rail steel. For comparison with the static case, it is convenient to define

$$K_R = \frac{\sigma_R}{c}\left(\frac{I}{2b}\right)^{\frac{1}{2}} \tag{A.19}$$

whereupon Equation (A.17) can be written as

$$K = K_R \left[1 - \frac{V^2}{V_{cr}^2}\right] \tag{A.20}$$

This is Equation (14) of the main text.

Equation (A.20) can be used to estimate the speed of steady-state dynamic crack propagation along the web of a rail through the use of the kinetic approach to dynamic fracture; i.e., Equation (2). In general, this would require a representation of the material dynamic fracture property. It can be heuristically assumed that K_{ID} is given by a relation like Equation (5). The equation governing the crack speed is then obtained by equating $K_{ID} = K_{Ia} + DV^m$ to K as given by Equation (A.20). Rearranging to have the terms containing the crack speed on the left hand gives

$$\frac{K_R}{V_{cr}^2} V^2 + DV^m = K_R - K_{Ia} \tag{A.21}$$

In general, unless m is an integer, an iterative solution of Equation (A.21) would be required. Two special cases are of interest. First, if m is taken equal to 2, for this instance Equation (A.21) can be readily solved to get

$$V = \left[\frac{K_R - K_{Ia}}{K_R/V_{cr}^2 + D}\right]^{\frac{1}{2}} \tag{A.22}$$

Finally, regardless of m, if D = 0, the result that is obtained is

$$V = V_{cr}\left[1 - \frac{K_{Ia}}{K_R}\right]^{\frac{1}{2}} \tag{A.23}$$

This is Equation (17) of the main text.